frontiers in Earth Science

ORIGINAL RESEARCH
published: 13 February 2018
doi: 10.3389/feart.2018.00011

Opal-A in Glassy Pumice, Acid Alteration, and the 1817 Phreatomagmatic Eruption at Kawah Ijen (Java), Indonesia

Jacob B. Lowenstern[1], Vincent van Hinsberg[2], Kim Berlo[2], Moritz Liesegang[3], Kayla Iacovino[1†], Ilya N. Bindeman[4] and Heather M. Wright[5]*

[1] Volcano Science Center, United States Geological Survey, Menlo Park, CA, United States, [2] Department of Earth and Planetary Sciences, McGill University, Montreal, QC, Canada, [3] Department of Earth Sciences, Freie Universität, Berlin, Germany, [4] Department of Earth Sciences, University of Oregon, Eugene, OR, United States, [5] Cascades Volcano Observatory, Vancouver, WA, United States

OPEN ACCESS

Edited by:
James D. L. White,
University of Otago, New Zealand

Reviewed by:
Bettina Scheu,
Ludwig-Maximilians-Universität München, Germany
Raffaello Cioni,
University of Florence, Italy

***Correspondence:**
Jacob B. Lowenstern
jlwnstrn@usgs.gov

†Present Address:
Kayla Iacovino,
Arizona State University, Tempe, AZ, United States

Specialty section:
This article was submitted to Volcanology, a section of the journal Frontiers in Earth Science

Received: 27 October 2017
Accepted: 30 January 2018
Published: 13 February 2018

Citation:
Lowenstern JB, van Hinsberg V, Berlo K, Liesegang M, Iacovino K, Bindeman IN and Wright HM (2018) Opal-A in Glassy Pumice, Acid Alteration, and the 1817 Phreatomagmatic Eruption at Kawah Ijen (Java), Indonesia. Front. Earth Sci. 6:11. doi: 10.3389/feart.2018.00011

At Kawah Ijen (Indonesia), vigorous SO_2 and HCl degassing sustains a hyperacid lake (pH ~0) and intensely alters the subsurface, producing widespread residual silica and advanced argillic alteration products. In 1817, a VEI 2 phreatomagmatic eruption evacuated the lake, depositing a widespread layer of muddy ash fall, and sending lahars down river drainages. We discovered multiple types of opaline silica in juvenile low-silica dacite pumice and in particles within co-erupted laharic sediments. Most spectacular are opal-replaced phenocrysts of plagioclase and pyroxene adjacent to pristine matrix glass and melt inclusions. Opal-bearing pumice has been found at numerous sites, including where post-eruption infiltration of acid water is unlikely. Through detailed analyses of an initial sampling of 1817 eruption products, we find evidence for multiple origins of opaline materials in pumice and laharic sediments. Evidently, magma encountered acid-altered materials in the subsurface and triggered phreatomagmatic eruptions. Syn-eruptive incorporation of opal-alunite clasts, layered opal, and fragment-filled vesicles of opal and glass, all suggest magma-rock interactions in concert with vesiculation, followed by cooling within minutes. Our experiments at magmatic temperature confirm that the opaline materials would show noticeable degradation in time periods longer than a few tens of minutes. Some glassy laharic sedimentary grains are more andesitic than the main pumice type and may represent older volcanic materials that were altered beneath the lake bottom and were forcefully ejected during the 1817 eruption. A post-eruptive origin remains likely for most of the opal-replaced phenocrysts in pumice. Experiments at 25°C and 100°C reveal that when fresh pumice is bathed in Kawah Ijen hyperacid fluid for 6 weeks, plagioclase is replaced without altering either matrix glass or melt inclusions. Moreover, lack of evidence for high-temperature annealing of the opal suggests that post-eruption alteration of pumice is more likely than pre-eruption envelopment of

euhedral opal-replaced phenocrysts in dacitic melt. At Ijen and elsewhere, the ascent of magma into hydrous acid-altered mineral assemblages (e.g., opal, kaolinite, alunite) could induce rapid dehydration of hydrous minerals and amorphous materials, generating considerable steam and contributing to magmatic-hydrothermal and phreatomagmatic explosions.

Keywords: pseudomorph, hyperacid, amorphous silica, opal-A, phreatomagmatic, pumice, volcanic lake, Kawah Ijen

INTRODUCTION

Acid alteration prevails at many volcanoes where shallow magma outgasses into a water-saturated edifice. Magmatic steam condensate forms and mixes with meteoric water encouraging intensive water-rock interaction and silicate hydrolysis, typically at high water-to-rock ratios (Christenson and Wood, 1993; Delmelle and Bernard, 1994; Africano and Bernard, 2000; Berger et al., 2014; Henley, 2015). Low pressures favor high SO_2/H_2S and HCl/NaCl in the emitted magmatic vapors, increasing the acidity of any near-surface condensate (Symonds et al., 1994; Shinohara, 2009). The creation of acid is further favored where crater lakes are present at the surface, as the supply of capping groundwater water minimizes the possibility that the gas-steam mixture can escape directly to the atmosphere (Delmelle et al., 2015). Such environments are highly analogous and indeed inseparable from the high-sulfidation environments responsible for some types of epithermal ore formation (Henley and McNabb, 1978; Hedenquist et al., 1998; Berger et al., 2014). In the most acid-altered areas, the dominant material is various forms of silica (Hemley and Jones, 1964; Henley and McNabb, 1978; Hedenquist et al., 1994; Delmelle et al., 2015), which may convert with time from amorphous silica (opal-A) to more crystalline forms of silica, including opal-CT, opal-C, chalcedony and quartz (Rodgers et al., 2004). Other minerals may include alunite, anatase, and kaolinite. Many such rocks contain >90% SiO_2, primarily because there is near-total dissolution of the rocks by the strong (mostly sulfuric) acid (Hedenquist et al., 1994; Hedenquist and Taran, 2013). Often termed "vuggy quartz" or "vuggy silica" rocks when exposed after uplift and erosion, they presumably originate from protracted water-rock reaction where residual silica remains, with or without associated sulfates such as alunite and barite (Hedenquist and Taran, 2013). Amorphous silica can also form during decompression and quenching of hot hydrous fluids in magmatic and hydrothermal environments at temperatures up to 400°C (Williamson et al., 2002; Tanner et al., 2015) or during cooling of silica-saturated waters in hot-spring environments (Fournier and Rowe, 1966; Rodgers et al., 2004). Occasionally, acid-altered rocks bearing amorphous silica are expelled directly from the subvolcanic environment during phreatomagmatic eruptions (Christenson and Wood, 1993; Wood, 1994; Christenson et al., 2010; van Hinsberg et al., 2010a; Mayer et al., 2015). In a study of erupted lake sediments from the Ruapehu (NZ) crater lake, Christenson et al. (2010) noted the presence of opal-A as replacement of plagioclase. Similar silica pseudomorphs were recently reported from hydrothermal eruptions at Mt. Ontake (Japan) in 2014 (Minami et al., 2016), phreatomagmatic events at Cotopaxi, Ecuador (Gaunt et al., 2016), and altered rocks from the Poás Crater in Costa Rica (Rodríguez and van Bergen, 2017). At Kawah Ijen, a variety of opaline ejecta were described from the 1817 phreatomagmatic eruption by van Hinsberg et al. (2010a). Acid altered, silica-dominated rocks are also found in outcrop in an area exposed by the 1817 explosions (Kemmerling, 1921; Delmelle and Bernard, 1994; Takano et al., 2004; van Hinsberg et al., 2010a; Scher et al., 2013).

Herein, we present a perplexing yet revelatory example of opaline materials within pumice, and laharic sediments from the 1817 phreatomagmatic eruption at Kawah Ijen. Most striking are opal-replaced phenocrysts (ORP) or pseudomorphs after euhedral plagioclase and pyroxene within otherwise fresh glassy pumice found at numerous localities around Ijen. In addition, micro-xenoliths of opal-bearing sediments are observed within fresh pumice and glassy laharic sediments from the 1817 eruption. We explore the pathways by which such materials can originate within volcanic materials. One clear implication is that the interaction of magma with hydrated, opaline silica may aid in triggering phreatomagmatic and magmatic-hydrothermal (*cf.* phreatic where both are defined in Browne and Lawless, 2001) explosions (see also Mayer et al., 2016).

GEOLOGY AND HYDROLOGY OF KAWAH IJEN VOLCANO

Volcanic History

Kawah Ijen is a small stratocone located at the eastern edge of the elliptical Ijen Caldera (18 × 14 km) in the Sunda arc in far eastern Java (**Figures 1a,b**). The caldera is of unknown age, bracketed by the youngest-dated pre-caldera deposit at 295 ka and the oldest-dated post-caldera deposit at 50 ka (Sitorus, 1990). Kawah Ijen post-dates caldera formation and much of its layered basalts and andesites appear to be younger than 24 ka (Sitorus, 1990).

The summit crater of Kawah Ijen volcano (∼1 km in diameter) hosts a 600 × 800 m crater lake (**Figure 1c**) of oxidized hyperacid brine (Woudstra, 1921; Delmelle and Bernard, 1994; van Hinsberg et al., 2010b). Direct degassing of magmatic sulfur and chorine gases contributes to highly acidic conditions: the pH of lake water commonly approaches 0 and the total chemical load is >100 g/l. The water is saturated with native sulfur, gypsum, barite, anatase, α-cristobalite, celestite, and amorphous silica (Delmelle and Bernard, 1994). Some lake water seeps through to form springs in the Banyu Pahit creek, which drains the volcano to the

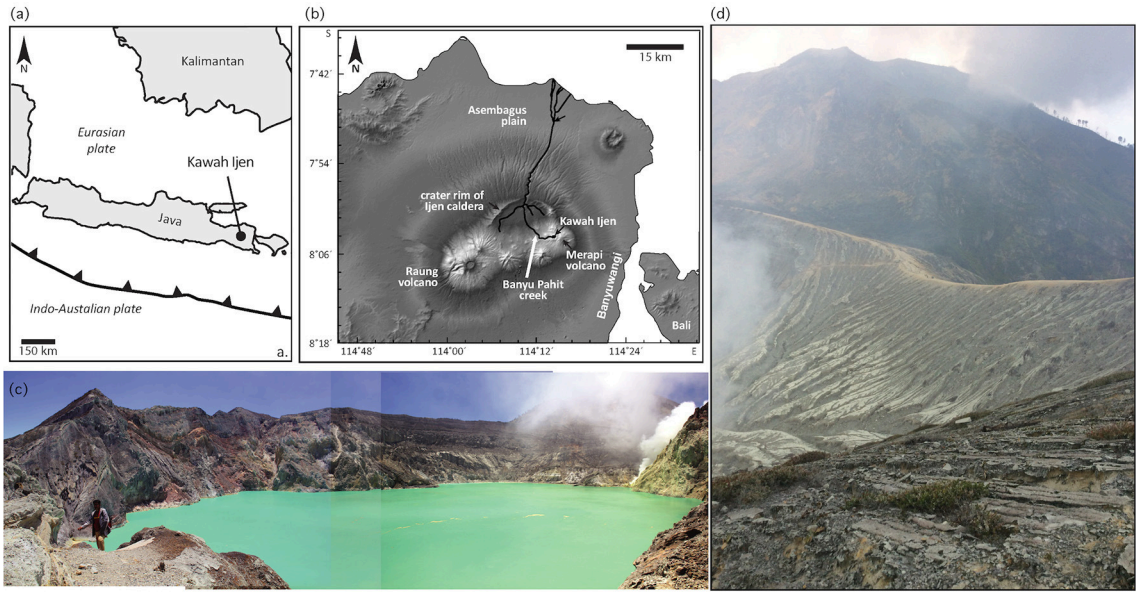

FIGURE 1 | Maps and photos of Ijen. **(a)** Map of regional location. **(b)** Digital elevation model of eastern Java. **(c)** Photograph montage of the highly acid Kawah Ijen crater lake, with active fumaroles to the right, and floating yellow sulfur mats visible. In this view, the lake is a maximum of 800 m in diameter. **(d)** Looking east from the south rim of Kawah Ijen crater, above and behind the fumaroles shown in **(c)**. As at many locations in and around the crater, incised muddy, pumice-bearing deposits from 1817 drape the inward-facing slopes.

west and then flows north (**Figure 1b**). Additional acid fluid is thought to reach these springs by direct emissions from the subsurface (acidic) hydrothermal system (van Hinsberg et al., 2015).

1817 Eruption

Some of the early history of exploration of the volcano was covered by Caudron et al. (2015), from which this summary of the recent history of Kawah Ijen is abstracted. Colonial visitors described the lake as early as 1789, and sulfur from the crater was used for the manufacture of gunpowder in the late 18th Century. A series of notable magmatic-hydrothermal and phreatomagmatic eruptions occurred during January and February 1817. Starting on January 16, earthquakes, explosions and a sun-blocking ash column could be felt, heard, and seen from the city of Banyuwangi, 20 km to the southeast. There was sufficient ash in town to collapse bamboo huts and topple trees. From around January 25 to February 5, cold mudflows laden with debris extended down drainages to the southeast, as well as through the Banyu Pahit out of the caldera and to the north across the Asembagus plain (**Figure 1b**). On February 10, another explosion followed and deposited 3–4 cm of dry gray ash in Banyuwangi. Presumably, this final burst provided the phreatomagmatic debris found coating the surface of the entire Kawah Ijen crater and deposited at the top of the lahar sediments found in the drainage of the Banyu Pahit. Caudron et al. (2015) concluded that the total erupted volume far exceeded any difference in crater size before and after 1817, and that a significant volume must therefore have erupted as magma.

Acid Altered Rock and Opaline Silica in Kawah Ijen Crater

van Hinsberg et al. (2010a) and Scher et al. (2013) described a ridge of acid-altered rock that represents the feeders of a solfatara system exposed in the 1817 eruption. Zones of residual silica, alunite-pyrite and dickite-kaolinite host high-sulfidation ore mineralization. Active fumaroles on a mound next to this ridge reach temperatures of 200–450°C. Scher et al. (2013) inferred that much of the mineralization formed due to water-rock reaction as magmatic gas condensed to form highly reactive acid fluids ∼100 m below the pre-1817 crater floor.

van Hinsberg et al. (2010a) described acid-altered rocks from three separate environments at Kawah Ijen: (1) the fumarolic solfatara found near the lake within the crater, described above, (2) where acid creek waters of the Banyu Pahit drainage directly infiltrate local wallrocks, and (3) the hydrothermal system beneath the lake. At all three locations, silicate minerals could be found fully leached and reacted to amorphous silica. Whole-rock analysis of altered rock reveals that they consist of >90% wt. SiO_2, with small proportions of residual Al_2O_3, Fe_2O_3, TiO_2, and ZrO_2 (van Hinsberg et al., 2010a,b; Scher et al., 2013; **Table 1**). Petrographic inspection and chemical analysis of variably altered basaltic lava flows in the Banyu Pahit revealed that the rock matrix was altered prior to plagioclase, followed by pyroxene (van Hinsberg et al., 2010a,b). Pyroxene alteration is similar in both clinopyroxene and orthopyroxene, and is not apparently controlled by crystal zoning. Moreover, in contrast with plagioclase, pyroxene zoning was found to consist of layered amorphous silica (Figures 4g,h of van Hinsberg et al., 2010a). van Hinsberg et al. (2010a) inferred that the matrix of basaltic

TABLE 1 | Whole-rock chemistry of 1817 pumice from Kawah Ijen.

Type	IJ-1L[&] pumice	IJ-2 pumice	IJ-3 pumice	KV99-851* acid-altered
	Normalized Major Elements (Weight %):			
SiO_2	64.55	66.63	61.32	93.85
TiO_2	0.873	0.787	0.764	1.024
Al_2O_3	14.24	13.88	16.74	2.21
FeO*	6.74	5.91	6.69	1.25
MnO	0.143	0.124	0.136	0.01
MgO	2.45	1.99	2.43	0.12
CaO	4.21	3.53	5.36	0.29
Na_2O	3.34	3.34	3.39	0.18
K_2O	3.29	3.63	3.00	0.62
P_2O_5	0.170	0.187	0.176	0.46
LOI	2.62	3.99	3.40	9.40
Original Sum	96.18	94.89	95.53	90.60
XRF	**Unnormalized Trace Elements (ppm):**			
Ni	5	6	7	20
Cr	3	4	4	
Sc	20	16	18	
V	148	106	146	54
Ba	670	705	614	1,141
Rb	88	97	80	31
Sr	286	242	351	45
Zr	212	240	195	282
Y	28	28	27	17
Nb	8.7	9.9	8.1	
Ga	16	14	17	4
Cu	12	20	31	168
Zn	66	57	63	20
Pb	17	34	19	
La	20	24	22	
Ce	41	40	43	
Th	12	15	10	31
Nd	22	20	23	
U	4	3	3	5
ICP-MS				
La ppm	22.22	23.09	21.58	
Ce ppm	44.55	46.04	43.06	
Pr ppm	5.48	5.54	5.32	
Nd ppm	21.83	21.93	21.30	
Sm ppm	5.04	5.02	4.90	
Eu ppm	1.09	1.05	1.21	
Gd ppm	4.87	4.76	4.72	
Tb ppm	0.83	0.82	0.80	
Dy ppm	5.06	5.03	4.89	
Ho ppm	1.07	1.06	1.02	
Er ppm	3.05	3.01	2.90	
Tm ppm	0.45	0.46	0.44	
Yb ppm	2.96	3.02	2.79	
Lu ppm	0.48	0.49	0.44	
Ba ppm	674	707	613	
Th ppm	10.29	11.60	9.54	
Nb ppm	8.89	9.55	8.08	
Y ppm	27.95	27.77	26.64	
Hf ppm	5.94	6.59	5.40	
Ta ppm	0.65	0.70	0.59	
U ppm	2.47	2.68	2.28	
Pb ppm	16.73	34.36	20.84	
Rb ppm	83.2	91.9	76.6	
Cs ppm	3.69	4.03	3.40	
Sr ppm	287	243	350	
Sc ppm	18.9	15.7	17.8	
Zr ppm	216	243	196	

*From van Hinsberg et al. (2010b). [&]Leached in deionized water prior to analysis. IJ-1L, IJ-2, and IJ-3 are pumice lumps in sample 15HW-IJ13.

lavas at Ijen was altered prior to phenocrysts, but it is possible that little if any glass existed in the slowly cooled lava flows they studied. However, melt inclusions in these basalts are observed to alter prior to their host plagioclase and pyroxene, which may indicate that relative susceptibility to alteration is controlled by glass composition.

Similar examples of vuggy silica alteration products are shown in **Figure 2** of this manuscript, including filled vugs (**Figure 2c**), and opal-replaced phenocrysts (**Figure 2d**). We use the term amorphous opal or amorphous silica in this manuscript as we can verify that much of the material is non-crystalline and deposited as nano-spheres of hydrous silica. Nevertheless, we cannot and have not verified that every example of suspected opaline material remains amorphous.

MATERIALS AND METHODS

In September 2015, gray-to-tan pumice lumps were sampled in the Banyu Pahit drainage below the lake/dam. The pumice lumps are most evident embedded in the muddy, cohesive, but non-lithified deposits where they form resistant tops to otherwise eroded columns of muddy matrix (**Figure 3a**). In addition, the pumice lumps are common "float" material found lying on the floor of the drainage, evidently derived from erosion of the lahar deposits (e.g., samples F1, F2, and WF3). Samples from float and samples obtained intact from the 1817 stratigraphy were sampled as part of this study, the latter from the lahar and from deposits on the volcano flank (e.g., KV14-102 and KV14-005: Figure S1).

The largest pumice lump observed was ∼30 cm in diameter, though more typical large lumps had a diameter of 5–15 cm. In the field, the pumice was described as having a glassy matrix with 5 to 15% of white tabular phenocrysts (**Figures 3b–d**), later identified as opaline pseudomorphs after (dominantly) plagioclase. Additional pumice lumps from the 1817 eruption

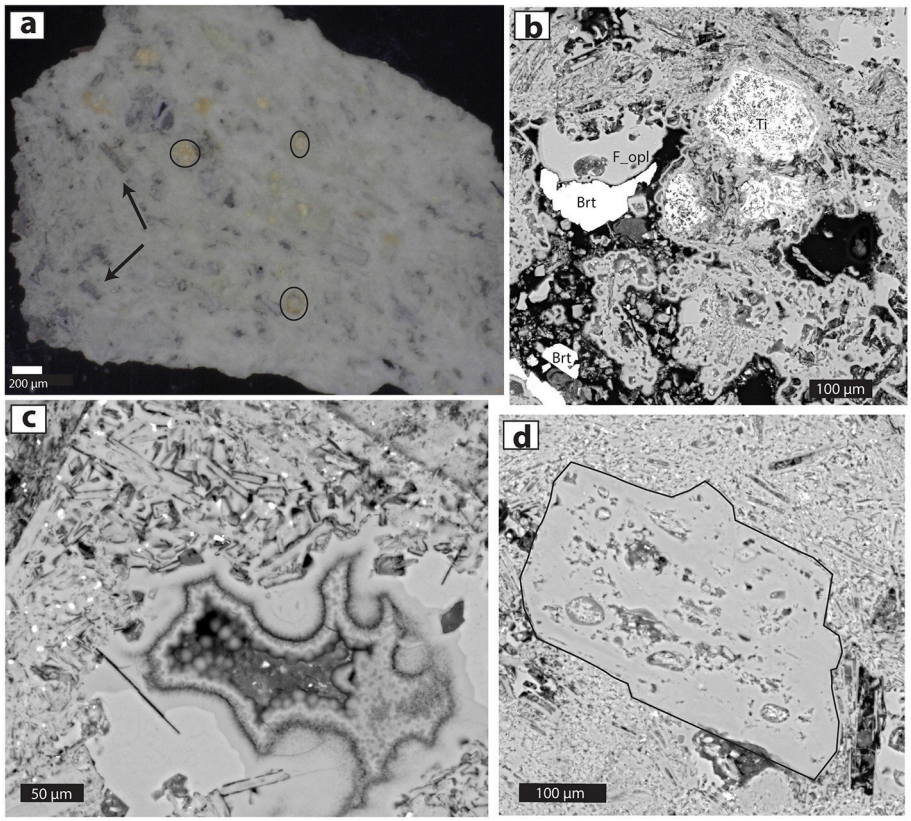

FIGURE 2 | Photomicrographs of acid-altered wallrock from Kawah Ijen (sample KV07-605). **(a)** Doubly polished slab (200 µm thick) of opaline rock with obvious lath-like ORPs (arrows), opal fragments (circled) and groundmass of micrometer-sized white colloidal particles. Photo with a stereo microscope. **(b)** BSE image of fine-grained porous opal, low-porosity opal infill (labeled F_opl), Ti-rich crystal remnants (Ti: originally titanomagnetite?) and barite infill (Brt). **(c)** Opaline vug fill shown in BSE image. All material is opal, including lath-like replacements of seriate feldspars, vuggy opaline infills, botryoidal opal agglomerations, and a few bright Ti-Fe oxide phases. Variation of grayscale of opal is due to differences in the density and/or H_2O content of the amorphous silica. **(d)** A 0.5-cm-diameter ORP (outlined in black) surrounded by opaline groundmass including much smaller laths of replaced feldspar microlites.

deposits had been collected previously by VvH and KB at a variety of locations around Ijen (Figure S1). Sediments from the 1817 lahar deposits were collected in September 2016 by P. Kelly of the USGS and Suparjan of the Ijen volcano observatory in the Banyu Pahit drainage (S 08.05749, E 114.23521) close to where the pumice lumps were also collected.

Samples of acid-altered rocks were obtained from the feeder system of the pre-1817 fumaroles as part of the studies of van Hinsberg et al. (2010a,b, 2015) . Sample KV07-605 is a jointed volcanic bomb or intrusive dike that has been leached by acid condensate in the subsurface rocks exposed during the 1817 phreatomagmatic eruption (**Table 1**, **Figure 2**).

Tabular pseudomorphs after plagioclase were hand picked from the sample, lightly crushed using an iron mortar, and were hand powdered using an agate mortar and pestle for XRD analysis. A Rigaku Multiflex X-ray diffractometer with Cu-Kα radiation (wavelength 1.54059 Å) with an accelerating voltage of 40.0 kV and a filament current of 20.0 mA measured the X-ray diffraction pattern of a randomly oriented powder mount at room temperature. The powder was scanned from 2° 2 θ to 70° 2 θ at a step size of 0.01° and scan speed of 1° 2θ per minute. Peaks, d-spacings, and intensity were determined using the program Theta.XRD version 1.1.

Fourier Transform Infrared (FTIR) transmission spectra were collected with a ThermoFisher Nicolet iN10-MX spectrometer at the USGS in Menlo Park. To prepare the delicate and porous opaline material, samples were impregnated with thermoplastic resin, doubly polished, and then dropped in acetone to dissolve the resin. Quantification of water in amorphous silica was achieved with extinction coefficients from Graetsch et al. (1985). One un-impregnated sample was re-analyzed after heating to 800°C in a Leitz 1350 heating stage, where temperature was increased at a rate of ∼50°/min prior to leaving at run-temperature for 30 min (Experiment Series 3 in the Discussion). The quench back to <100°C was achieved in 1 to 2 min.

Raman spectroscopy analyses were conducted on a Horiba Jobin Yvon LabRAM HR 800 intrument coupled to an Olympus BX41 microscope at the Museum für Naturkunde (Berlin, Germany). A 785 nm air-cooled diode laser was used to excite the sample with a 100x objective, a spectral integration time of 60 s, and 3 accumulations. With the Peltier-cooled (−70°C) CCD detector (1024 × 256 pixels), a spectral resolution of ∼0.2

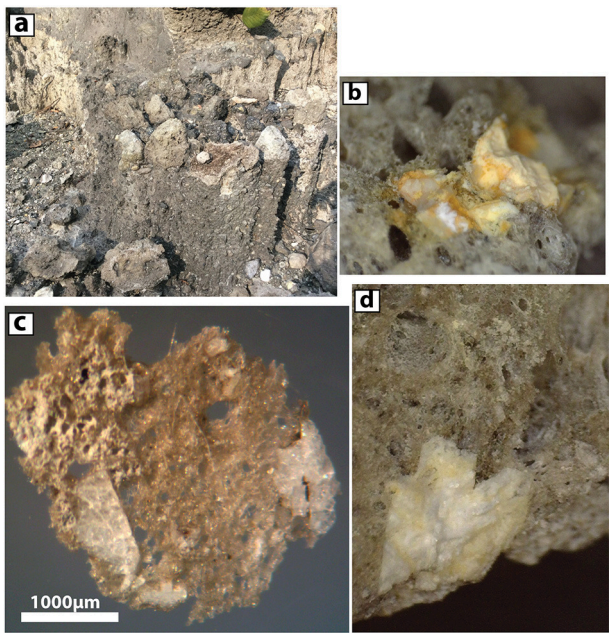

FIGURE 3 | Characteristics of Ijen 1817 pumices. **(a)** In the field, gray dacite pumice lumps are found near the top of gravelly lahar deposits. Largest lumps in this image are ∼10–20 cm in diameter. **(b)** Binocular dissecting microscope image of opaline detritus in pumice lump. Field of image is ∼3 mm across **(c)**. Stereo microscope image of doubly-polished pumice and included opal-replaced phenocrysts (ORPs). **(d)** Stereo microscope image of pumice and a feldspar ORP (cream-colored material at bottom). Image is 4 mm across.

cm^{-1}/pixel is achieved. Scattered Raman light was collected in backscattering geometry and dispersed by a grating of 600 grooves/mm after passing through a 100 µm entrance slit. The confocal hole size was set to 1,000 µm. Unpolarized spectra were collected with the Labspec 6 software over a range from 100 to 1,200 cm^{-1}. An internal intensity correction (ICS, Horiba) was used to correct detector intensities. The instrument was calibrated using the Raman band of silica at 520.7 cm^{-1}.

Electron microprobe analyses of glass, phenocrysts, alteration minerals and opaline material were performed using a JEOL 8900 with a 15 kv beam running at 5 nA with a 5 µm spot (glass) and 10 nA focused beam (opal, alunite). Standards included a variety of mineral and glass specimens in common use at the USGS Menlo Park microprobe facility and were analyzed at the same sample conditions.

Backscattered electron (BSE) images were collected on the Menlo Park Tescan Vega scanning electron microscope (SEM) using a focused 30 kV beam and current between 10 and 20 nA. Polished sections were typically coated with sputtered carbon, whereas unpolished grain mounts were coated in Au or Au-Pd. Elemental maps, mineral identification, and semi-quantitative analysis were undertaken by means of the Energy Dispersive Spectroscopy (EDS) detector. The micromorphology of amorphous silica in opal-replaced phenocrysts was investigated by SEM in Berlin. In this case, specimens were etched in 10 vol% HF solution for 15 s, dried, and sputter-coated with ∼15 nm W. Secondary electron images were obtained with a Zeiss Supra 40 VP Ultra SEM instrument, at an acceleration voltage of 5 kV and beam current of 10 nA.

Bulk samples of pumice and separates of opaline silica were analyzed for δD and wt. % H_2O with a TCEA-MAT 253 system at the University of Oregon Stable Isotope Lab as discussed by Nolan and Bindeman (2013). The $\delta^{18}O$ analyses of bulk perlite was performed in 1–2 mg quantities using laser fluorination using a home-built airlock chamber allowing analysis of a single sample without prefluorinating other samples. Bromine pentafluoride was used as a reagent with liquid N_2 traps and a mercury diffusion pump used to strip away excess fluorine. Released oxygen was converted to CO_2 using a hot graphite filament following procedures described in Bindeman (2008) and Loewen and Bindeman (2015) and analyzed relative to an in-house standard of Gore Mountain Garnet (UOG = 6.52‰). Errors are 0.1‰ based on replicate analysis of standards.

Experiments (Series 1 and 2) to determine the stability of ORP were performed in vertically mounted cold-seal pressure vessels (pressurized with H_2O) at isothermal and isobaric conditions of 750, 800, or 850°C and 2, 20, or 75 MPa at Stanford University. Between 30 and 70 mg of chips of opal-bearing Ijen pumice was loaded into 3 and 4 mm Au capsules, which were crimped and welded shut at both ends. One experiment (IJ-04) was seeded with opal by adding small (∼1 mm) chunks of Ijen ORP. No water was added to the 2 and 20 MPa experiments; 3 wt.% H_2O was added to the 75 MPa experiments. H_2O pressure was raised to 40 MPa before heating the sample to run temperature at a rate of ∼30°C min^{-1} via an external tube furnace. Pressure was then raised or lowered to final run conditions. Temperature was measured with a sheathed chromel-alumel thermocouple (K-type) located close to the sample capsule. All experiments were run for 24 h and then quenched by removing the pressure vessel from the furnace and spraying with room temperature compressed air until the sample reached ∼200°C. This resulted in an average quench rate of ∼200°C min^{-1} or a quench time of approximately 3 min.

Alteration experiments (Series 4) were conducted on 5 × 5 × 10 mm cut blocks of fresh Kawah Ijen 1817 pumice, submerged in 10 mL of Banyu Pahit hyperacidic fluid enclosed in a welded glass tube. One experiment was kept at 100°C in a convection oven, whereas the other was in a room regulated to 25 ± 5°C. The pumice blocks were removed after 6 weeks, washed in nanopure water, dried, sectioned and embedded in resin. This time was chosen to ensure adequate time for equilibration at room temperature (near ambient for surface temperatures at Ijen). The coated polished surfaces were BSE imaged on a JEOL 8900RL microprobe at McGill University at 15 kV and 10 nA, and analyzed using EDS.

RESULTS

Petrography of 1817 Pumice

All Ijen pumices contain 10 to 30% phenocrysts (the remainder is glass), and vesicularities typical for pumice (on the order of 70%). Gravimetric study of a single pumice lump indicated a bulk density of 0.66 g cm^{-3}, indicating an apparent porosity of ∼73%. Fresh phenocrysts consist of orthopyroxene, clinopyroxene, and

Ti-magnetite. Some samples have abundant fresh plagioclase, though more typical are opaline pseudomorphs after feldspar, reminiscent of those seen in **Figure 3d** from acid-altered rock (discussed below in the next paragraph), and some samples have both fresh and altered plagioclase. Apatite, pyrrhotite, and Cu-Fe sulfide were identified as inclusions in fresh phenocrysts. Barite was identified in a few vesicles, though most vesicles were empty. Two pumice lumps were analyzed for major and trace elements (**Table 1**). A third was leached in Nanopure water and then prepared for whole-rock analysis with the others (IJ-1L). All three analyzed 1817 pumice lumps are consistent with published Kawah Ijen fresh rock compositions (Sitorus, 1990; Handley et al., 2007; van Hinsberg et al., 2010b) with a depletion in, most notably, Ca, Na, K and Al resulting from partial alteration. The whole-rock pumice is significantly higher in FeO* and MgO than the matrix glass as analyzed by electron microprobe (**Table 2**), and lower in SiO_2, implying that oxide and pyroxene phenocrysts in the pumice have a strong effect on its bulk composition. The leachate rinse dissolved 0.25 wt.% of the pumice sample and yielded a S/Cl of 2 (by mass), indicating that some soluble material has been precipitated on the pumice during or after eruption.

After preparing the Ijen pumice lumps as thin sections, it became clear that the ubiquitous tabular white phenocrysts (**Figures 3b–d**) were highly atypical for normal volcanic rocks. They resemble feldspars in hand sample, but their poor polish in reflected light causes them to stand out from the glass and crystalline phases (**Figure 4b**). Moreover, between crossed polars, this phase is isotropic (**Figure 4d**). X-ray diffraction patterns of the material show a broad band centered at 22.5°2 θ consistent with amorphous silica (Jones and Segnit, 1971). Diffractograms also record several sharp peaks with low intensity and a prominent peak at 27.9°2 θ (Figure S2).

The typical Raman spectrum of opal-replaced pseudomorphs is also shown in Figure S2. The general pattern consists of prominent bands at about 482, 811, and 971 cm^{-1}. Previous studies assigned the Raman bands near 482 and 811 cm^{-1} to fundamental vibrations of the SiO amorphous silica framework (McMillan, 1984; King et al., 2011), while the band at 971 cm^{-1} indicates a Si-OH stretching mode due to silanol groups (Hartwig and Rahn, 1977). The spectra we obtained are basically identical to that obtained by King et al. (2011) for amorphous silica pseudomorphs after olivine, formed in highly acidic fluids.

Microprobe analysis demonstrates that the X-ray amorphous tabular phase is composed almost entirely of SiO_2, with substantial (5–30%) summation deficits (**Table 2**, Table S1). Silica alteration within incipiently altered feldspars contains a higher proportion of Al_2O_3, with some samples exceeding 4 wt.% (Table S1). Variations in backscatter intensity correlate with summation deficit, consistent with low totals due to high total water (H_2O + OH) or low density/high porosity of the opaline material. FTIR and TCEA analyses indicate that the material contains substantial (2–4 wt.%) H_2O (Table S2), but not tens of percent. This implies that the porous nature of the opal contributes to the low totals (see additional discussion below). As discussed below, high-resolution secondary electron imaging confirmed a porous arrangement of sub-micrometer-sized amorphous silica spheres.

Though plagioclase was present in some pumice lumps, more typically, the only evident plagioclase was relict and located in the interior of opal-replaced plagioclase (e.g., **Figures 4b–d**, **5**). Similarly, both orthopyroxene and clinopyroxene could be found in the interiors of "zebra-striped" pseudomorphs (**Figure 4e**; Figure S3). Similar textures were noted by van Hinsberg et al. (2010a) in their study of acid-altered rocks from Kawah Ijen. Though both pyroxenes and plagioclase have been replaced by opaline silica, their textures are markedly different (**Figure 4e**). Feldspar is replaced by massive opal, whereas pyroxene is replaced with sheet-like layers of opal that are readily infiltrated by epoxy when the pumiceous samples are vacuum-impregnated with epoxy resin prior to sectioning. An important additional observation is that some fresh phenocrysts and microlites of orthopyroxene and clinopyroxene are common in all pumice. Fresh plagioclase is rare in most samples, but is identified in others, including the core of a breadcrust bomb. Opaline replacement of phenocrysts was identified in the majority of samples of 1817 pumice.

For convenience, we refer to all "phenocrysts" of opal-A as *opal-replaced phenocrysts* (ORP) to clarify that they are not crystalline but their morphology clearly reflects replacement of igneous phases. ORP are bordered almost invariably by a sharp contact with fresh rhyodacitic matrix glass (**Figures 4a,e**, **5**). There is no evidence of reaction between the glass matrix and the opal except in very rare cases (e.g., **Figure 4f**). The glass is pristine, with no evidence of secondary hydration, and has chemistry typical of evolved melt from Kawah Ijen (van Hinsberg et al., 2010a, **Table 2**). Inclusions of glass are common within the ORP-plagioclase, and have compositions similar to the matrix (**Figure 6**, **Table 2**).

ORP are visible at sizes and scales ranging from 10 μm to 10 mm within the sample. *Euhedral* tabular ORP as small as 5–10 μm can be spotted within the glassy matrix. Rarely, opaline replacements after feldspar were "anhedral" and appeared to be unstable compared with more euhedral ORP (Figure S4). The ORP-feldspar are 4 to 5 times more common than the striped ORP-pyroxenes, plausibly representing the prevalence of feldspar in unaltered dacite. As mentioned above, fresh pyroxenes and oxides are present in all 1817 pumice, sometimes closely adjacent to ORP. In some samples, fresh plagioclase is also evident next to ORP-plagioclase.

We could not identify pathways for acid migration through the pumice. Few cracks are visible and very few minerals are present in vesicles that would testify to migration of a fluid. One breadcrust bomb did contain a dense core that contained solely unaltered phenocrysts, and this was used for the alteration experiments (Series 4). There was never any evidence for directional flow of migrating fluid or reaction fronts within the pumice.

TABLE 2 | Electron microprobe (EPMA) and SEM data for glass, minerals, opal and other materials.

Spot #	**MgI11**	**MgD61**	**MgD63**	**MgD65**	**MgE81**	**MmD51**	**MmI7**	**MmH35**	**MmH37**	**MmH39**	**MmB109**
Date	**11-Jan-16**	**11-Jan-16**	**11-Jan-16**	**11-Jan-16**	**11-Jan-16**	**11-Jan-16**	**11 Jan-16**	**11-Jan-16**	**11-Jan-16**	**11-Jan-16**	**11-Jan-16**
Sample	**F1**	**F1**	**F1**	**F1**	**F1**	**F1**	**F1**	**F1**	**F1**	**F1**	**F1**
SiO2	66.81	67.60	67.32	67.53	67.50	67.89	67.41	68.60	68.99	68.32	67.26
TiO2	0.65	0.55	0.53	0.69	0.63	0.62	0.67	0.59	0.58	0.70	0.68
Al2O3	14.41	14.55	14.41	14.46	14.96	14.42	13.64	14.15	14.26	14.20	14.73
FeO	3.71	3.81	3.43	3.48	3.76	3.70	3.86	3.03	3.00	3.07	3.83
MnO	0.10	0.11	0.13	0.05	0.14	0.10	0.08	0.10	0.11	0.10	0.09
MgO	0.82	0.76	0.71	0.78	0.83	0.90	0.92	0.63	0.57	0.53	0.75
CaO	2.36	2.34	2.05	2.29	2.49	2.00	2.00	1.82	1.72	1.74	2.25
Na2O	3.97	3.93	4.11	4.31	4.21	3.82	4.16	3.96	3.85	3.81	3.81
K2O	5.06	5.00	5.16	4.94	5.18	5.13	5.06	5.25	5.40	5.44	5.03
Cl	0.17	0.18	0.15	0.16	0.15	0.13	0.18	0.18	0.18	0.17	0.18
Total	98.33	97.99	97.19	97.80	98.92	97.86	97.06	97.43	97.78	97.10	97.66
Type	Matrix glass EPMA	Matrix glass EPMA	Matrix glass EPMA	Matrix glass EPMA	Matrix glass EPMA	Included glass EPMA	Included glass EPMA	Included glass EPMA	Included glass EPMA	Included glass EPMA	Included glass EPMA
Spot #	**MmE77**	**MmB107**	**86**	**88**	**90**	**KV07-605_45**	**MsD70**	**MSC92**	**MSC93**	**MSC98**	**46**
Date	**11-Jan-16**	**11-Jan-16**	**24-Feb-16**	**24-Feb-16**	**24-Feb-16**	**17-Jan-2017**	**11-Jan-16**	**11-Jan-16**	**11-Jan-16**	**11-Jan-16**	**12-Jun-17**
Sample	**F1**	**F1**	**F1**	**F1**	**F1**	**KV607-605**	**F1**	**F1**	**F1**	**F1**	**F1**
SiO2	68.86	67.15	53.15	52.48	52.04	84.02	91.98	93.12	94.07	91.08	2.98
TiO2	0.51	0.63	–	0.41	0.36	0.31	–	–	–	–	0.26
Al2O3	14.44	14.74	0.66	1.79	1.60	2.71	0.07	0.19	0.05	0.47	55.17
FeO	2.80	3.62	22.58	8.89	11.26	–	0.00	0.00	0.06	0.03	0.02
MnO	0.11	0.09	–	0.46	0.41	–	–	–	–	–	0.01
MgO	0.54	0.75	21.87	16.32	14.33	–	0.00	0.00	0.00	0.04	0.00
CaO	1.88	2.04	1.74	19.65	19.66	–	0.02	0.01	0.00	0.01	0.05
Na2O	4.27	4.24			0.33	–	0.11	0.13	0.03	0.09	0.75
K2O	5.09	5.08				–	0.04	0.06	0.04	0.12	4.57
SO3	0.17	0.15				–	–	–	–	–	40.49
Total	97.87	97.61	nd	nd	nd	87.04	92.22	93.50	94.25	91.83	108.00
Type	included glass EPMA	included glass EPMA	opx SEM	cpx SEM	cpx SEM	ORP EPMA	ORP EPMA	ORP EPMA	ORP EPMA	ORP EPMA	Alunite(?) EPMA

EPMA, Electron microprobe; SEM, scanning electron microscope; opx, orthopyroxene; cpx, clinopyroxene; ORP, opal-replaced phenocryst included glass is glass found within ORP, whereas matrix surrounds the ORP.

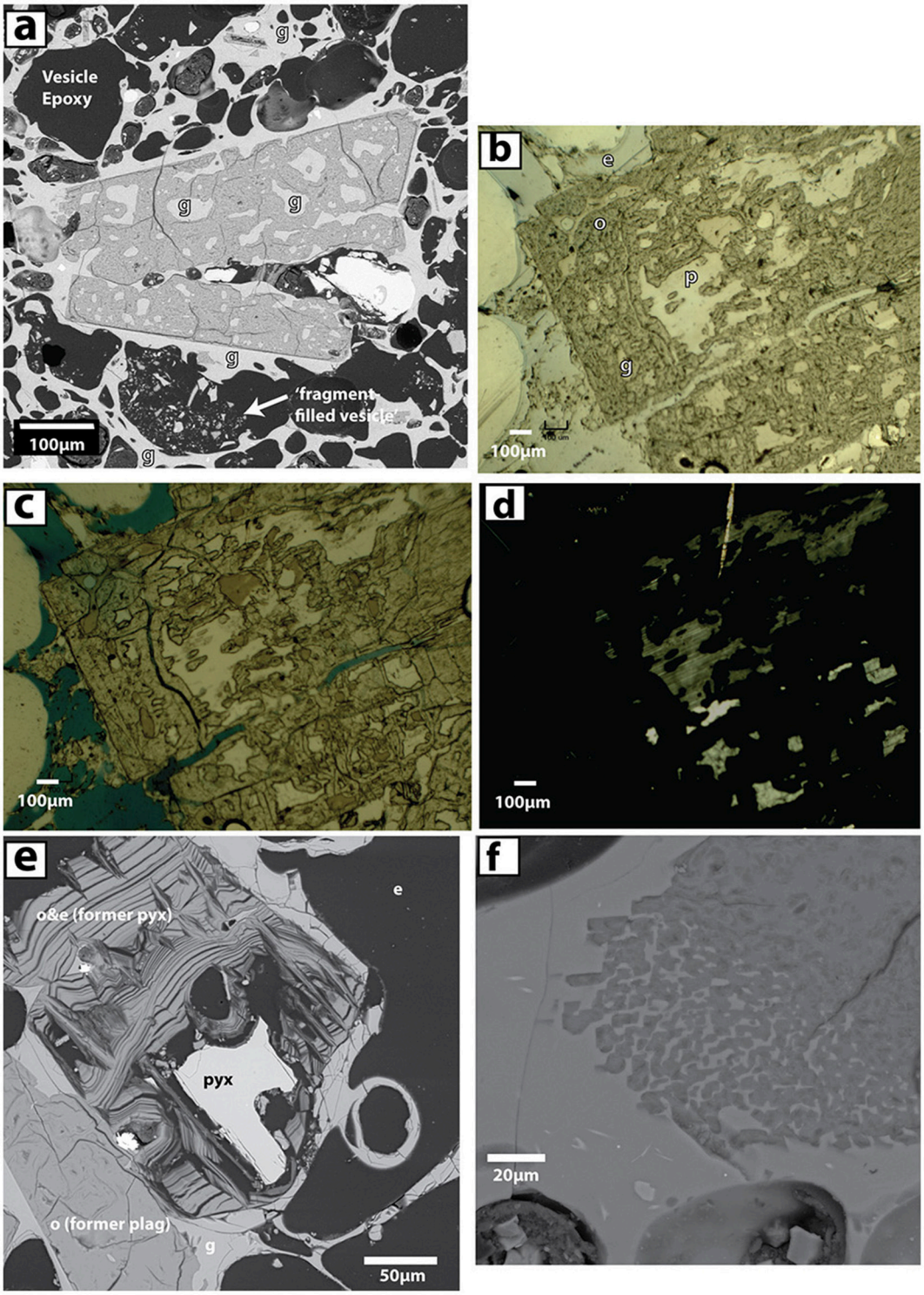

FIGURE 4 | Opaline phases in 1817 pumice (F1) from Kawah Ijen. **(a)** BSE image of seemingly euhedral ORP with habit of plagioclase. Glass (g) is evident as both inclusions within the opal phase and as pumiceous groundmass in sharp contact with this and other apparent phenocrysts. A fragment-filled vesicle is shown toward the bottom of the image and contains shards of pumiceous glass and opal. **(b)** Reflected light image of ORP (poorly polished) containing plagioclase (p) and included glass (g). Epoxy (e) fills most vesicles and cracks within the phenocrysts. **(c)** Transmitted light image of **(b)** Epoxy is now blue. The glass is browner than the plagioclase remnant phenocryst (white). The opaline material is dusky gray. **(d)** Transmitted light image with crossed polars. Plagioclase shows birefringence, while opal, glass, and epoxy are isotropic and light does not pass through the section where they reside. **(e)** BSE image where opal fully replaced plagioclase (lower left) but partially replaced pyroxene. The remnant pyroxene (both orthopyroxene and clinopyroxene are present in pumice) sits within a zebra-striped texture with alternating sheets of opal and void (filled with epoxy). Such textures are absent in replaced feldspars. **(f)** BSE image of prismatic silica phase found in pumice. Discussed in text.

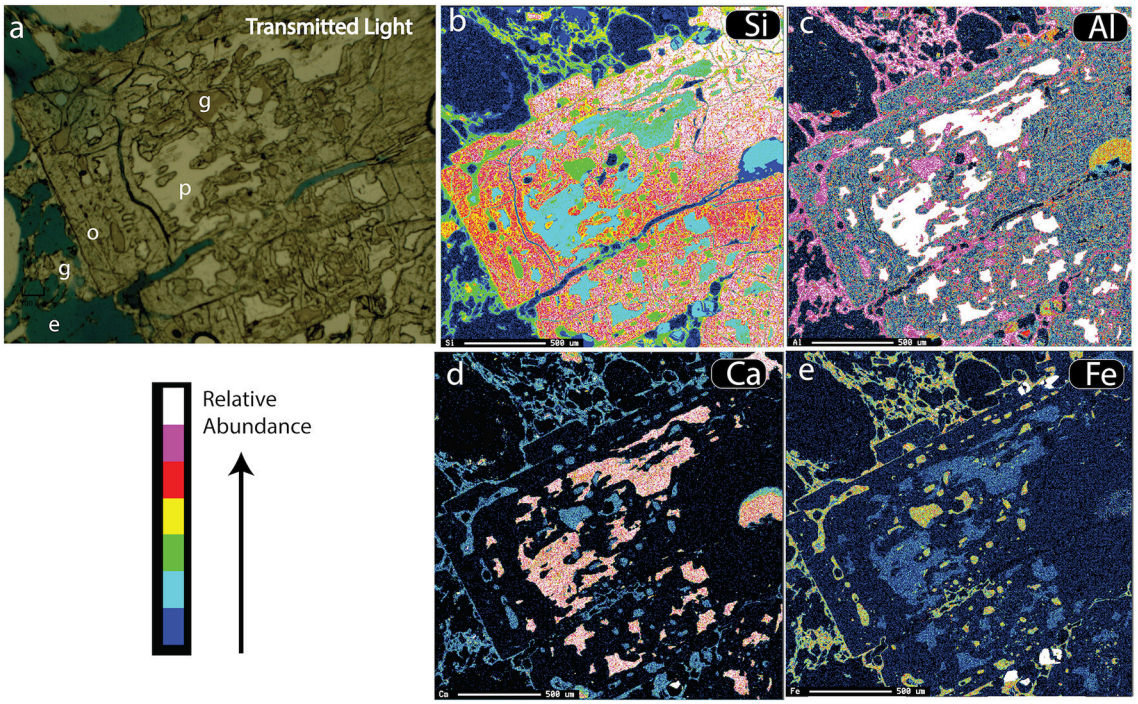

FIGURE 5 | Maps of ORP (originally plagioclase feldspar) in pumice (F1). **(a)** Transmitted light image showing glass (g), blue-tinted epoxy (e), opaline silica (o) and relict plagioclase (p). **(b)** SEM-created element map of Si counts, highlighting opal (red/yellow). **(c)** Similar map of Al counts, **(d)** Map of Ca counts, which highlights plagioclase (pink). **(e)** Map of Fe counts, which highlights yellow matrix glass and glass inclusions.

Additional Opaline Material in Ijen 1817 Pumice

Besides the ORP present within the 1817 pumice, opaline and other non-volcanic material was found as fragments within the pumice (**Figure 7**). Some opaline pieces contained layers of 10–20-μm-sized opaline spheres, which presumably originated as colloidal particles or aggregates thereof (**Figures 7a,b**). Variations in their backscatter intensity (especially **Figure 7b**) could originate from variations in H_2O or sample density. As with the ORP, EPMA analyses indicate that the layered opal consisted of >95% SiO_2, with only minor amounts of Al_2O_3 (typically <2 wt.%) and TiO_2 (<0.5 wt.%). However, summation deficits reached values up to 30%, in the grayer areas of **Figure 7b**, most likely due to a combination of H_2O and high micro-porosity of the opal (see discussion below). Uncommon clasts of opaline sediment were also found enveloped in fresh pumiceous glass as in **Figure 7c**, or as large chips within vesicles or glass (Figure S5). In some samples, hydrothermally altered lithics were found that contain alunite or clay-like material interpreted to be kaolinite (Figure S5b).

An additional common texture in the pumices are fragment-filled vesicles (**Figure 4a**). The resident 1- to 15 μm particles are dominated by fragments of dacite glass similar to the pumice matrix as well as fragments of opaline silica. The supplement shows two examples of such fragment-filled vesicles: one that fills a vesicle (Figure S6) and one that borders it and appears to have been displaced or deformed at the time of final vesicle expansion (Figure S7).

Lahar Sediments in the Banyu Pahit

Grain mounts of sieved separates from the 1817 Banyu Pahit laharic sediments contain ∼10% glass-absent grains similar to the opal-replaced volcanic rocks in **Figure 2**, or intergrowths of opaline silica and alunite (Figures S8–S10). Much more common are glassy fragments that range in composition from andesite to rhyodacite and are generally more mafic than glass found within the 1817 pumice (**Figure 6**). Within the glassy fragments, ORP are omnipresent, and include pseudomorphs after plagioclase and pyroxene with various degrees of alteration from incipient to complete (Figures S12–S14). As with the examined pumice, fresh phenocrysts can be located adjacent to wholly replaced ORP. Occasional glassy grains are connected to cemented aggregates of opal and glass fragments (Figure S11).

Ten-to-twenty percent of glassy grains contain 50- to 150-μm-sized opal-rich, cemented aggregates (**Figure 7d**, Figures S14, S15). Vesicles commonly appear to have grown on these small xenoliths. Amongst the μm-sized sediment particles, we identified glass, opal, alunite, Fe-oxide, Ti-bearing (anatase?) and unidentifiable alteration minerals. These aggregates were differentiated from the fragment-filled vesicles within the pumice lumps (**Figures 7c,d** vs. Figure S6) due to their more integrated/cemented character and lesser (or absent) glass.

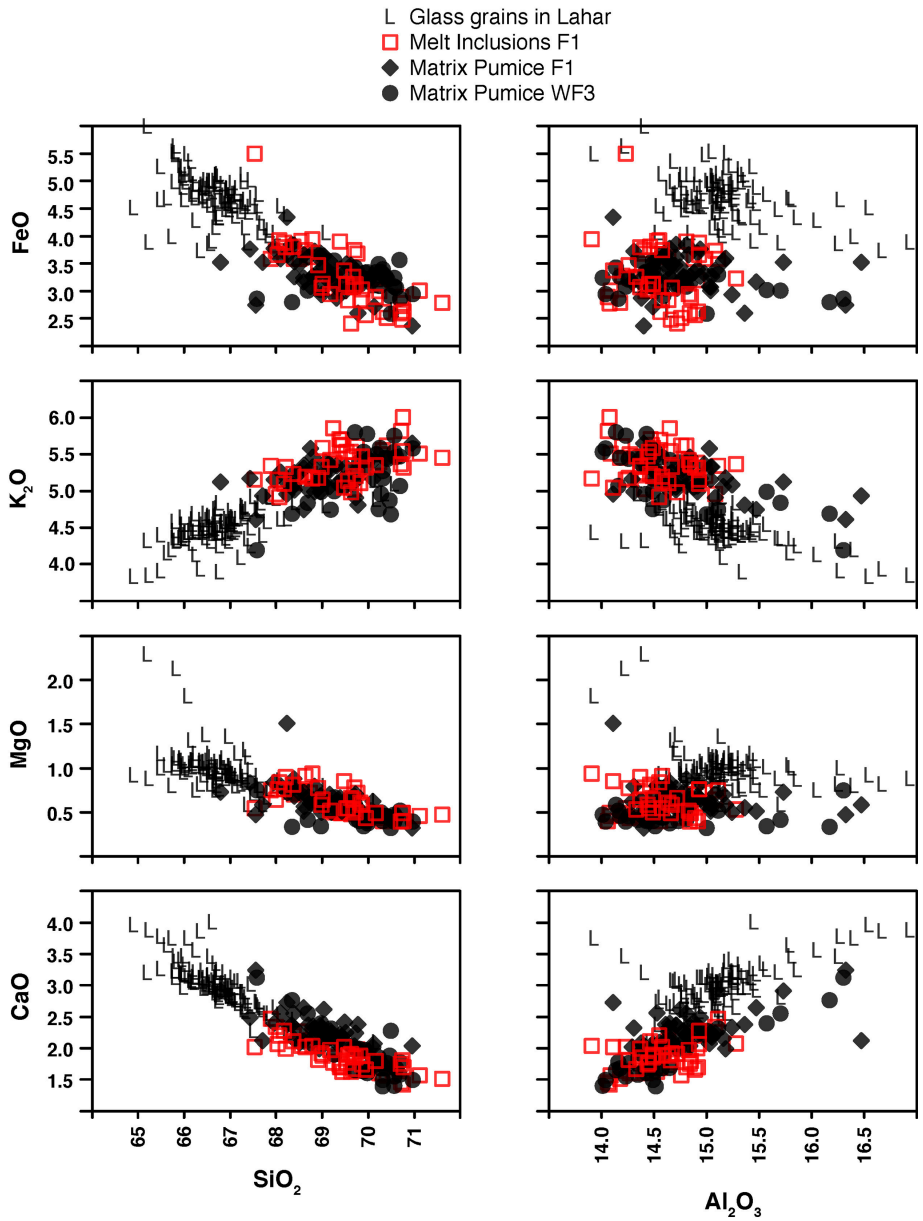

FIGURE 6 | Scatter plots for microprobe data for wt.% SiO_2 and Al_2O_3 vs. CaO, MgO, K_2O and FeO. Glass chemistry of matrix from two different pumice lumps (F1 and WF3) are shown as black diamonds and circles. Inclusion glasses (red squares) overlap the chemistry of the matrix. Glass analyses of ORP-bearing glassy grains in the 1817 lahar deposits tend toward more mafic compositions than the large pumice lumps that also erupted in 1817.

High-Resolution SEM Examination of ORP Textures

Scanning electron microscopy on thin (30 μm) and thick (~200 μm) sections of Ijen 1817 pumice reveals a series of remarkable textures (**Figure 8** and Figures S16–S18) that confirm that the ORPs consist of layers of opaline spheroids with an average diameter of ~40 nm. **Figure 8a** presents an overview of an entire ORP, including relict plagioclase and opal, in contact with pumiceous glass. The relict plagioclase forms a series of remnant feldspar islands within the opaline matrix. In **Figure 8b**, one can discern the fine structure within the white box of **Figure 8a**. Cracks border parallel planar sheets of opaline silica. Similar textures were noted in amorphous silica pseudomorphs after olivine created during leaching experiments with strong sulfuric acid (King et al., 2011). As in that study, a gap can be seen between the replaced crystal and the encroaching silicification front. This gap represents the most-recent reaction front, where acidic fluid replaced feldspar with layered opaline silica. We infer that most of the epoxy-filled lineaments within the ORP represent cleavage cracks or the

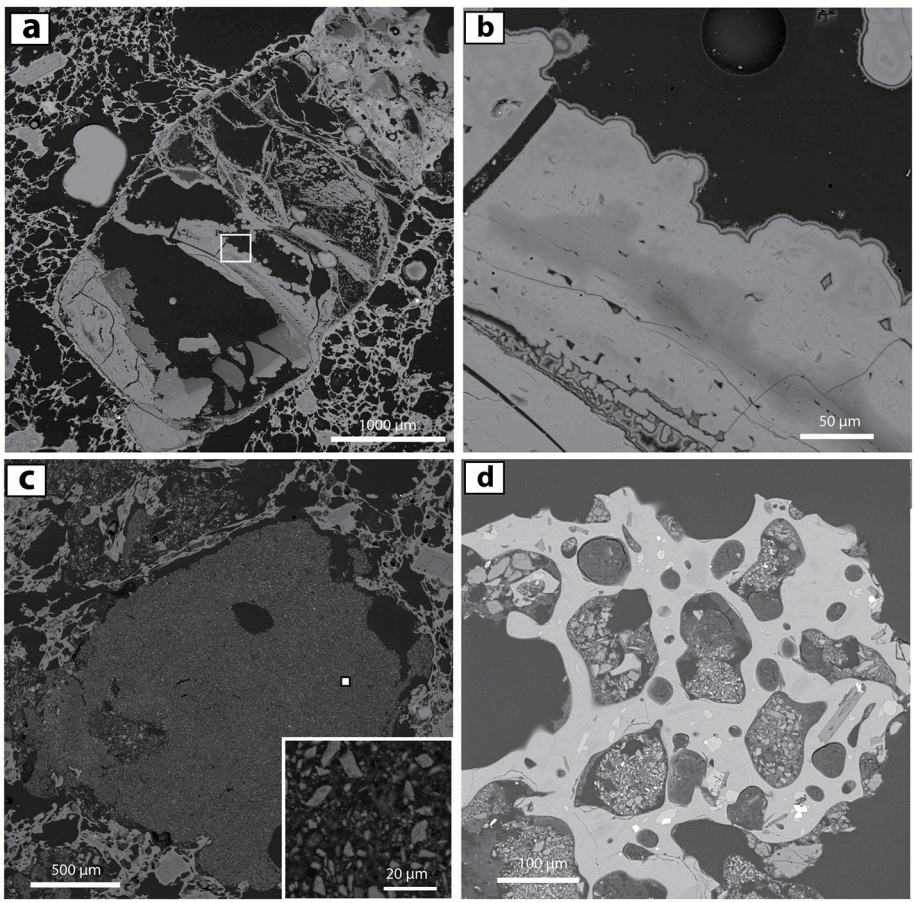

FIGURE 7 | BSE images of non-phenocryst-related opaline material in 1817 pumice and laharic deposits. **(a)** Large clast of layered colloidal opal, partly shattered, and adjacent to ORP-bearing vesicle-depleted material (upper right) in pumice F1. **(b)** Close-up of white box from **(a)** Variations in grayscale correspond to differences in opal density and/or H_2O content. **(c)** Micro-xenolith or aggregate of opal-rich sediment (>1 mm) within pumice (WF3). This lithic material was incorporated inside the pumice during the 1817 eruption. A small inset provides a closeup of a sample of the lithic (small filled white square). **(d)** Sedimentary micro-xenoliths within vesicles in 0.5 mm glassy grain from the 1817 Banyu Pahit lahar deposits. These opal-rich aggregates are dominated by 1- to 20-µm-sized altered particles. See text for further discussion.

migrated replacement fronts that originally began as cracks in the phenocrysts.

The annotated asterisk in **Figure 8b** sits left of a triangular infilling of opaline layers that probably formed by progressive replacement of a triangular plagioclase relict similar to that seen in the upper center of the figure part. Though most of the amorphous silica seen in **Figures 8b,d,e** is relatively dense, and composed of ∼30 to 50 nm-sized silica spheres, other regions of the ORPs are characterized by more porous opaline structures (**Figure 8c**, Figures S16, S18). We infer that the low microprobe totals of some opaline areas correlate directly with the high porosity of opaline regions within the ORP and other opaline materials found in the 1817 Ijen eruptive products.

Experimental Heating of 1817 Pumice

Experiment Series 1: Hydrous amorphous silica is normally thought to be unstable at magmatic temperatures (Graetsch et al., 1985), so discovery of opal-A in otherwise fresh pumice is confounding. We explored the thermal stability of these Ijen pumices by heating them to magmatic temperatures at variable confining pressures for 24 h (see Methods). For all evaluated conditions, the post-experiment ORPs were notably degraded, cracked, pitted, and void-bearing (**Figures 9b–d**). Whereas the ORP in fresh pumice contain abundant internal pockets of melt as in **Figure 9a**, remnant ORP after the experiment were riddled with voids (**Figure 9d**). The experiments also caused the groundmass to partly crystallize in all situations, even with the H_2O added in the experiments at 75 MPa.

Experiment Series 2: This experiment was performed with powdered andesite, chips of opal (sample KV07-605, shown in **Figure 3**) and 2 wt.% added H_2O at 900°C and 86 MPa. The experiment was intended to explore whether hydrous ORP-rich materials disaggregate and vesiculate when in contact with molten andesite at magmatic temperatures, thus providing numerous distributed opaline microlites and phenocrysts as seen in the natural samples. The sample was heated for 45 min and

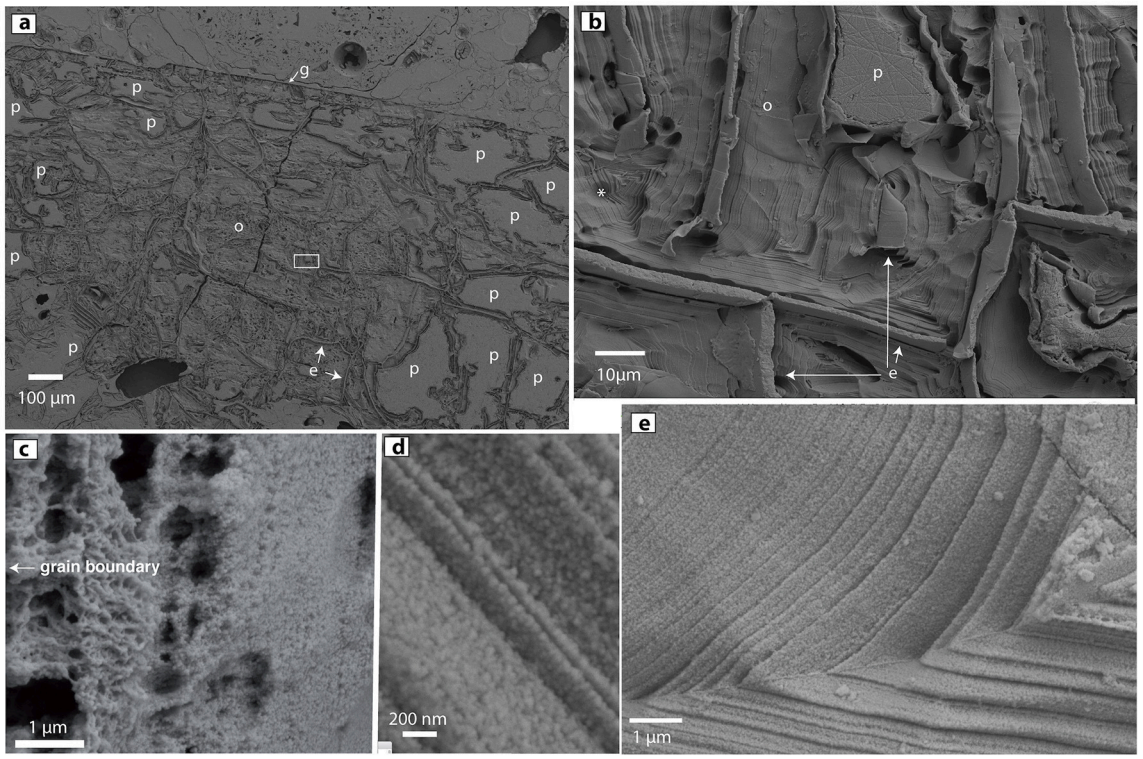

FIGURE 8 | High-resolution secondary-electron images of ORP in HF-treated thin sections. **(a)** ORP with highly eroded/etched opal (o), unaffected relict plagioclase (p), epoxy (e) and pumiceous glass (g). Small white rectangle is magnified in **(b)** Layers of opal nanoparticles align parallel to epoxy-filled cleavage cracks. The cracks apparently served as conduits for acid migration during opal replacement of the plagioclase phenocryst. The * at left is adjacent to an infilled triangular region that may have originated as a progressively replaced triangular feldspar fragment similar to that labeled (p). **(c)** Variations in opal porosity can be seen in this sample. Similar variations likely correlate to backscatter intensity and microprobe totals. **(d)** Close-up of layering of 40 nm-sized opaline nanospheres. **(e)** Fine layering of opaline nanoparticles.

left at temperature for 30 min. After the experiment, the opal chips remained intact and showed no evidence for inflation, comminution, or disaggregation.

Experiment Series 3: Another experiment was undertaken with a single ORP grain placed at ambient pressure in a Leitz 1350 fluid-inclusion heating stage. The sample was heated at a rate of 50°C per minute up to 800°C and left for 30 min before a rapid quench to ambient temperature in ∼5 min. FTIR analysis (**Figure 10**) revealed a radical loss in total water compared with a pre-heating spectrum of the same grain. The peak area at 3,500 cm^{-1} was reduced by a factor of ∼40, such that if the sample started with 3 wt.% H_2O, it was reduced to <0.1 wt.% during the hour-long experiment. Moreover, the peak transformed from very broad, and consistent with liquid water in amorphous material (Day and Jones, 2008), to a narrow band consistent with a small amount of structural OH^- within crystalline silica created from the opal during the experiment (see also Graetsch et al., 1985). Between crossed polars, inspection under the petrographic microscope revealed some birefringence in the post-experiment ORP, whereas ORP in the original Ijen samples were were always isotropic, implying that some of the opal may have converted to a more crystalline silica polymorph.

Acid-Pumice Reactions at Low- to High Temperature

Experiment Series 4: To explore whether post-eruption infiltration of hyperacid Kawah Ijen waters could allow for replacement of phenocrysts yet preservation of pumiceous glass, unaltered 1817 Ijen pumice was reacted with Banyu Pahit creek water for 43 days at 25°C. Similar experiment at 100°C were intended to explore similar reactions at the bottom of the lake, or slightly beneath the lake. In the 25°C experiments, plagioclase was incipiently replaced by opaline silica. In the 100°C experiments, the conversion of plagioclase to opal was nearly complete, pyroxene conversion was underway, and both matrix and inclusion glass remained pristine (**Figure 11**). Reconnaissance microprobe inspection indicated that silica concentrations were lower (and deficits were higher) than in the natural samples, consistent with higher water contents in the experimentally created opaline silica than in the natural samples.

Experiment Series 5: In a final experiment, dense fresh Kawah Ijen dacite was heated to 800°C at 86 MPa with Banyu Pahit water in a gold capsule for 3.5 h to investigate fluid-rock interaction at magmatic temperatures. No alteration of phenocrysts or glass was observed, but the groundmass was partly crystallized as also observed in experiment series 1.

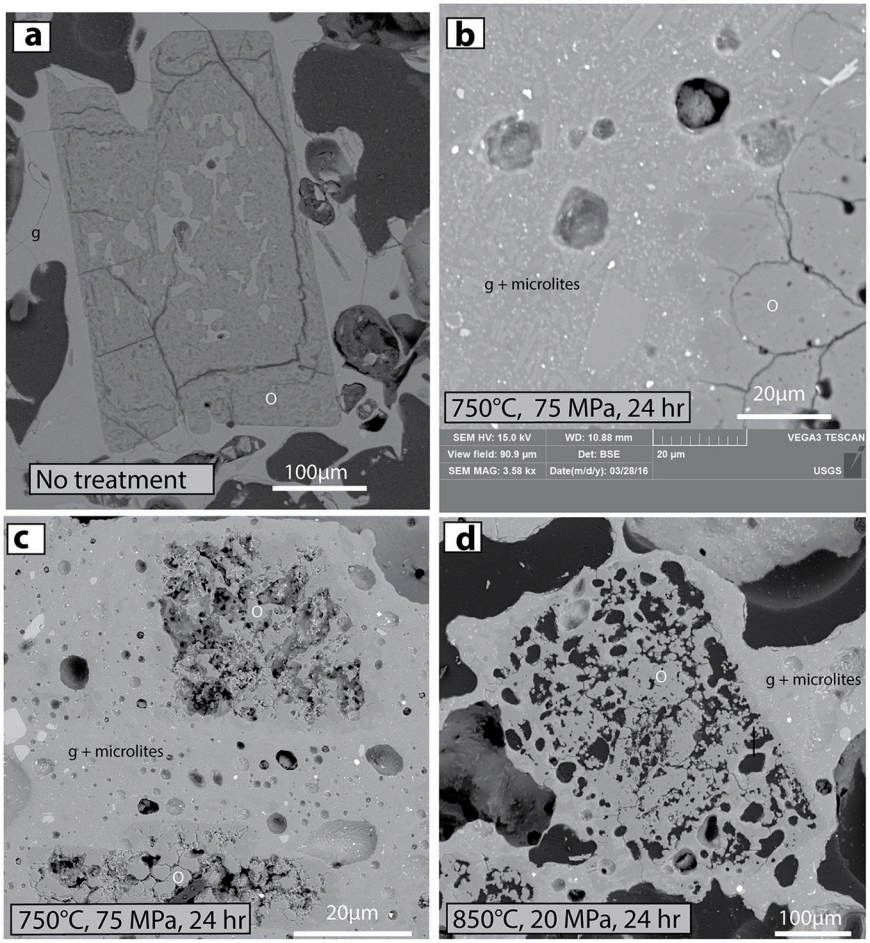

FIGURE 9 | BSE images that demonstrate effects of high-temperature experimental heating on stability of ORPs. **(a)** Untreated ORP in original thin section of Ijen 1817 pumice. ORP labeled as o, matrix glass is g. **(b)** Matrix glass of hydrated 1817 pumice has started to crystallize after 24 h at 750°C and 75 MPa. Microlites of plagioclase feldspar (light gray) and orthopyroxene (brighter gray) are labeled g + microlites. **(c,d)** ORPs are unstable, vuggy and partly crystallized to quartz after 24 h at two different pressure and temperature conditions. Three percent H_2O was added to the experiments at 75 MPa.

Stable Isotope and TCEA Analysis

Chips of ORP were hand picked from pumice and analyzed for $\delta^{18}O$ and δD (**Table 3**, **Figure 12**). They were very low in δD and very high in $\delta^{18}O$ compared with typical magma or volcanic gas compositions (**Figure 12**: green box). Local hot springs plot along the meteoric water line at δD of $-50 \pm 5‰$. Crater lake waters sampled at the surface have signatures consistent with warm evaporation of local rain to raise δD to ~ 0 and positive values of $\delta^{18}O$. Fumarole samples are intermediate between arc volatiles, the crater lake and local meteoric water (data from Delmelle et al., 2000, and van Hinsberg et al., 2015). The Ijen pumice (whole rock: labeled PUM in **Figure 12**) is similar to estimated silicic magma compositions, but slightly lower in δD, consistent with degassing of D-rich magmatic water (Dobson et al., 1989).

The bulk concentration of H_2O in the separated ORP as measured by TCEA (**Table 3**) ranges from 1.9 to 5.5 wt.%, consistent with FTIR analysis using extinction coefficients as in Day and Jones (2008). Such H_2O concentrations are consistent with opal-A studied from geyser discharge aprons (Graetsch et al., 1985), but are slightly low as might occur if the samples have lost some water due to dehydration.

DISCUSSION

Primary Observations

We used a variety of analytical methods and conducted experiments to clarify the origin of the opaline materials found in 1817 pumice and laharic sediments from Kawah Ijen. Many of our observations are contradictory, and few of them are completely definitive in ruling out potential pathways by which the ORP and opaline xenoliths found themselves in glassy pumice (**Table 3**). Prior to listing likely hypotheses for formation of the opaline materials, we review some of the key observations.

1) Acid-alteration is common at Ijen, and creates deposits rich in amorphous opaline silica at the surface, beneath the lake, and in the shallow volcanic plumbing system (Kemmerling, 1921; Delmelle et al., 2000; Takano et al., 2004; van Hinsberg et al.,

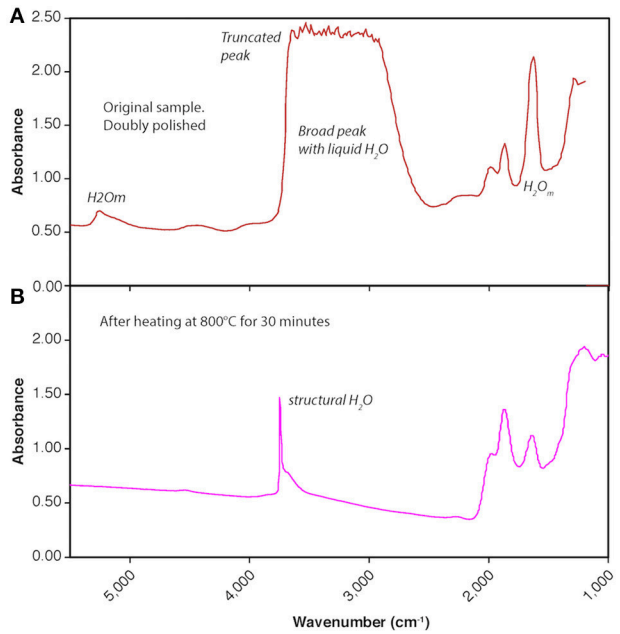

FIGURE 10 | FTIR transmission spectra before and after experimental heating of doubly polished ORP (250 μm thick). **(A)** Initial sample has abundant molecular H_2O evident in FTIR peaks at 1,630, 3,500, and 5,200 cm^{-1}, as well as limited hydroxyl (OH^-) at 4,500 cm^{-1}. The broad peak at 3,300–3,700 cm^{-1} is truncated due to an overabundance of water absorbers in the 250 μm sample thickness, indicating at least 2 wt% H_2O. **(B)** After experimental heating at atmospheric pressure and 800°C for 30 min, the sample is dehydrated, and most of the remaining water (<0.25 wt.%) is present as structurally bound OH^-, indicated by the narrow peak at 3,750 cm^{-1}, presumably reflecting incorporation of remaining water in a crystalline form of SiO_2 (most likely quartz).

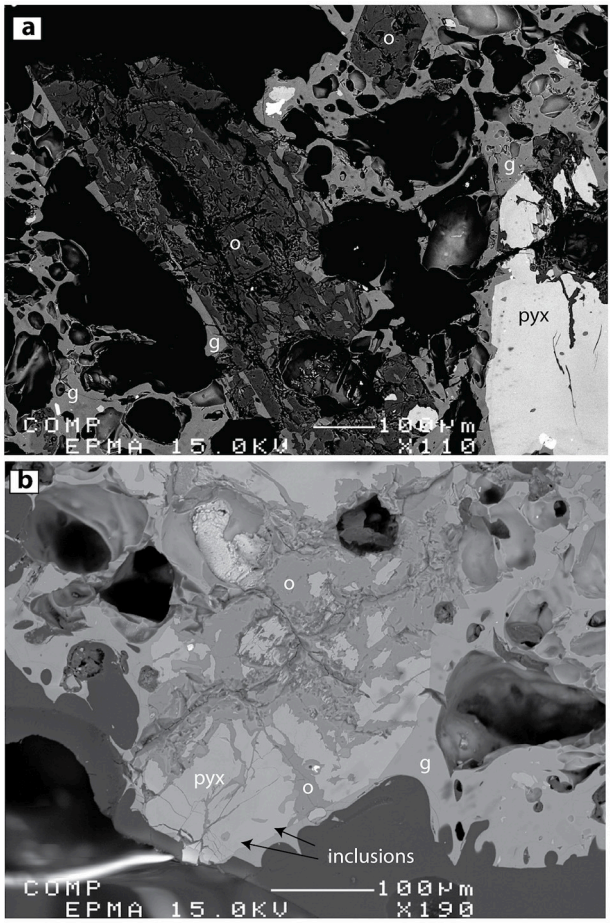

FIGURE 11 | BSE images of alteration products created during reaction of Ijen pumice (initially non-ORP-bearing) with Banyu Pahit creek water (~ pH 0) for 6 weeks at 100°C (Experiment Series 4). **(a)** Plagioclase (p) is almost completely converted to opaline silica (o). Matrix glass and melt inclusions remain unaltered. **(b)** Under the same conditions, pyroxene (pyx) alteration is initiated but not complete. Glass inclusions are evident toward the bottom of the image (arrows).

2010a; Scher et al., 2013). Opaline materials are likely to be encountered by rising magma at a variety of locales within the volcanic edifice.

2) Opal-A cannot survive at magmatic temperatures for more than a few tens of minutes, and will dehydrate and convert to more crystalline forms (**Figures 9**, **10**). At geothermal temperatures (150–250°C), its preservation is only temporary as it will ultimately convert to more thermodynamically stable phases (Herrington and Wilkinson, 1993; Lynne et al., 2006; Tanner et al., 2015).
3) ORP are common within pumices and glassy particles within laharic sediments from the 1817 eruption of Kawah Ijen. In most samples, plagioclase is either completely or partially replaced to opaline silica. Some pyroxenes are altered in most samples, though in most observed pumices, fresh pyroxenes and plagioclase can be found adjacent to ORPs of pyroxene and plagioclase. No obvious fluid pathway such as fractures in the groundmass were observed adjacent to OPRs, nor does the glass appear to be affected by fluid interaction. Most pumices contain ORP everywhere and not simply at the pumice edge.
4) Our experiments have confirmed that Banyu Pahit creek water reacts with low-silica dacite pumice and converts plagioclase and pyroxenes to opaline silica without initially reacting with the matrix glass or oxides (**Figure 11**). At the volcano, such alteration could occur within the volcanic plumbing system, at the bottom of the crater lake, or at the surface of the volcano wherever acid gains access to volcanic materials. Similar results were shown by McCollom et al. (2013) for interaction of strong sulfuric acid with basaltic scoria.
5) Only rarely did we observe any reaction between melt (now glass) and ORP. Contacts are sharp between ORPs and glass (e.g., **Figures 4a,b,e**, **5**, **9a**). No gradients in chemical composition were observed in the glass adjacent to the ORP compared with further away. Because quartz is not stable in this low-silica dacite, it would seem unlikely that opaline silica would be resistant to immediate contact with any infiltrating melt at magmatic temperature. Moreover, opal/melt contacts were degraded during experiment series 1 and 2, where materials were held at magmatic temperatures and pressures for 24 h. In the original pumices, there are a few

TABLE 3 | Potential origins of opaline materials in 1817 eruption products.

Type of opaline-bearing material	Composition	Origin A	Origin B	Origin C	Origin D	Examples
		Pre-eruptive assimilation into magma	**Syn-eruptive incorporation into magma**	**Eruption in 1817 of "cold" acid-altered materials**	**Post-eruptive alteration at ambient temp.**	
ORP: Replaced phenocrysts in pumice and glassy grains in laharic sediments	Amorphous silica, relict plagioclase, and pyroxene	Minor	Possible	Possible for laharic sediments	**Probable in pumice**	Figures 3b–d, 4a–e, 5, 8, Figures S3, S6, S7, S16–S18
Opaline fragments, and layered clasts in pumice	Amorphous silica	Unlikely	**Most Probable**	Unlikely	Unlikely	Figures 7a–c, Figure S5
Fragment-filled vesicles in pumice	Uncemented accumulation of fragments of dacite glass, amorphous silica, and rare sulfides	N/A	**Syn-eruptive formation most probable**	Very unlikely	Very unlikely	Figure 4a, Figures S6, S7
Cemented alunite-opal aggregate grains in lahar	Various ratios of the two materials.	Not applicable	Not applicable	**Most Probable**	Very unlikely	Figures S8–S10
Cemented, opal-rich aggregates in glassy grains of laharic sediments	Opal, glass, Ti-oxide, and unidentified materials	Not applicable	**Likely, enveloped in andesitic melt prior to 1817 eruption and stored in or beneath lake**	**Likely erupted as cold particles in 1817**	Very unlikely	Figure 7d, Figures S14, S15

Origins in bold are favored by the authors.

examples of ORP that have textures consistent with heating and dissolution of opal (e.g., **Figure 4f**). It is conceivable, though, that this skeletal texture represents granophyric feldspar (or quartz) that was replaced with amorphous silica, and not a euhedral ORP that has reacted with high-temperature melt. At this time, we cannot confidently rule out either possibility. We do note that a very few ORP within pumice do resemble those present after the high-temperature experimental runs (e.g., Figure S4 compared with **Figures 9b,c**).

6) Using fractionation factors from Kita et al. (1985), the observed range of 20 ± 8‰ $\delta^{18}O$ is consistent with formation of amorphous silica from meteoric water at 20°C, or with the heavier Kawah Ijen lake water (or magmatic water) at more elevated temperatures around 100–150°C. The low δD is consistent with dehydration and loss of H_2O from the opal at some point after initial formation as D is preferentially lost during silicate devolatilization (Dobson et al., 1989; Nolan and Bindeman, 2013). It is possible that a more detailed in-situ study of stable isotopes might identify multiple populations of opaline materials formed under disparate conditions.

Potential Origins for Opal-Bearing Eruption Products

Below, we present four primary options for origins of the opal-bearing materials found in the 1817 phreatomagmatic deposits. None of these can satisfactorily explain all the above observations, and reality may consist of a combination thereof. We then separately consider which origins are most likely for various 1817 eruptive products discussed above.

Origin A; Pre-eruption assimilation. Altered opal-bearing rocks are ingested into high-temperature igneous melt immediately prior to the 1817 eruptions.

Origin B; Syn-eruptive incorporation. Altered opal-bearing rocks are swept into the magma during the 1817 eruption. Some comminution of opaline material would occur during this process.

Origin C; Expulsion of "cold" acid-altered sub-lacustrine glassy sediments and pumice. Non-juvenile glassy detritus is thrown out from beneath the lake during the magmatic-hydrothermal and/or phreatomagmatic activity in 1817.

Origin D; Post-eruption alteration. ORPs and some other opaline materials in 1817 eruption products were created post-eruption by acid infiltration at ambient temperature (∼25°C).

ORP within Low-Silica Dacite Pumice Lumps

Our initial inspection of ORP in otherwise young, glassy pumice led us to strongly suspect that subvolcanic alteration products had been incorporated directly into ascending low-silica dacite melt (i.e., origin A). Origin A is supported by the common presence of unaltered pyroxenes, and in some cases plagioclase, within a few tens of microns of partially, or wholly replaced ones. Potentially, fresh pyroxene-bearing magma incorporated opal-bearing altered rocks, accounting for the near association of fresh and altered materials.

However, two factors argue against origin A, at least in regard to the great preponderance of ORP. First, our experiment

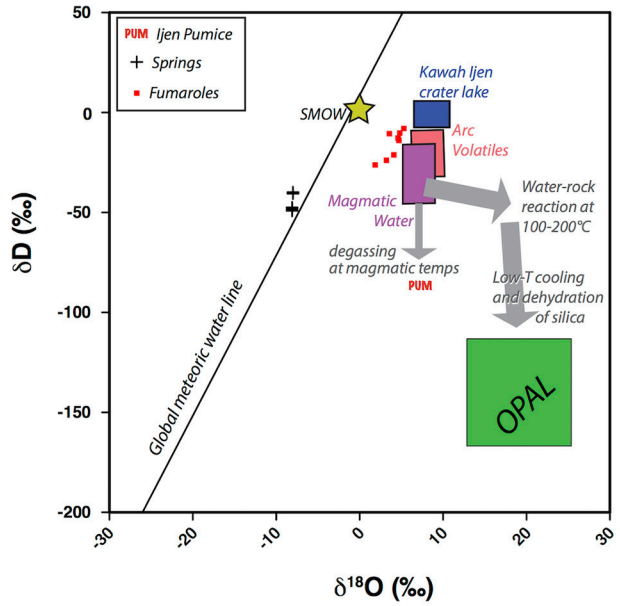

FIGURE 12 | δD vs. $\delta^{18}O$ for diverse materials from Ijen. The green opal box represents the range of δD and $\delta^{18}O$ found for various ORP fragments. Box for the Kawah Ijen crater lake and regional springs from Delmelle et al. (2000). Kawah Ijen fumaroles from Delmelle et al. (2000) and van Hinsberg et al. (2015). Boxes for magmatic water and arc volatiles from Hedenquist and Lowenstern (1994). Ijen pumice (PUM) is consistent with loss of D through eruptive degassing. Stable isotope composition of opal are radically different than meteoric waters or acid lake water. The low δD can be explained by low temperature dehydration (pre- or post-eruptive) of amorphous silica, wherein fractionation (loss of D) is more extreme as temperature declines.

series 1, 2, and 3 demonstrate that the opal breaks down at magmatic temperatures, and H_2O would be lost from the opal within a few tens of minutes. The ORP we studied contain more water than should be present after heating to 800°C (experiment series 3). Second, Raman spectra and most of the SEM images (**Figure 8**) showed no evidence for sintering or re-crystallization of the opaline nanospheres, as would be expected during heating. Again, some ORP are vuggy and may have a different origin, but others contain opaline layers consistent with phenocryst replacement at ambient or low hydrothermal (<100°C) temperatures (King et al., 2011).

There remain a few examples of potential temperature-degraded opal that might have been incorporated into dacite magma prior to the eruption of 1817 (**Figure 4f** and Figure S4), and then thermally degraded. However, origin A appears to have been a minor factor in contributing opaline materials to the 1817 eruption deposits. More likely, some ORP could have been swept into the melt during the magmatic climax to the 1817 eruption (origin B), but it is difficult to conceive of how the opal-replaced materials could be stored in the subsurface, and distributed into a magma without considerable physical or thermal degradation. It seems most likely that the dominant population of the pristine-looking ORP were formed post-eruption by infiltration of acid (origin D). Origin D is supported by experiment series 4, which demonstrated that we can synthesize ORP of plagioclase and pyroxene at one-to-two month timescales and ambient temperatures without affecting the silicic glass, including melt inclusions (see also McCollom et al., 2013). Acid fluid might have migrated through the pores and fractures of pumiceous materials and sediments, selectively replacing those phenocrysts and sediments with which it interacted.

Because the pumice is highly inflated, and found mostly as erupting late within the 1817 stratigraphy, we do not favor Origin C, where the pumice would be erupted as cold material after vesiculation, quenching, and alteration beneath the lake. Origin D is the simplest origin for most ORP, though the mode of post-eruption acid infiltration into the pumice remains poorly understood (addressed below).

Opal-Bearing Lithic Materials within 1817 Pumice

Unlike the ORP, however, there are a variety of opaline materials within Ijen pumice lumps that appear most consistent with origin B, syn-eruptive incorporation of acid-altered, opal-bearing materials. Specifically we refer to clasts of opal that reflect laminar growth and sedimentary textures that would be unlikely to form during post-eruptive infiltration of acid. Examples are highlighted in **Figures 6a–c**. We observed a ∼5-mm-long piece of layered opaline silica in 1817 pumice (**Figures 7a,b**) that shows unidirectional growth toward the upper right of both figure parts. The opal is not filling a void in the pumice, which would show a concentric structure. Another example of a sedimentary aggregate in pumice is shown in **Figure 7c**. It is entirely surrounded by glass, and retains a cohesive texture as if it was incorporated into the melt prior to or during eruption. Other fragments of opal-bearing aggregates within pumice are shown in Figure S5.

A final example of potential syn-eruptive incorporation of opal in pumice consists of the fragment-filled vesicles (Figures S6, S7). These common features are composed of fragments of dacitic glass and opal. Their location, and the highly fragmental nature of the glass and opal implies that these features were formed during vesiculation. We did not observe opal-absent examples, but always a mixture of opal and glass fragments. We suspect that they formed due to comminution of the cold, hydrous opaline alteration products during infiltration and inflation of dacite melt. Occasionally, they appear deformed during later vesiculation (Figure S7). A similar process might be eruption of the dacitic magma through a slurry of water and opaline fragments, similar to what can occur in Surtseyan eruptions where magma is erupted through a glassy slurry such that ash fragments are enveloped by growing vesicles (e.g., Schipper and White, 2016). Perhaps magma fragmentation creates ash particles that mix with existing sediments (opal) and are incorporated into the expanding magma. For these materials, Origin B seems far more likely than any post-eruption alteration unless the opal fragments replace phenocryst fragments formed during syn-eruptive vesiculation. In such an example, the fragment-filled vesicles would form during vesiculation, but would experience acid alteration after eruption.

Glass-Free Laharic Sediments

There is little doubt that the glass-free, 100% opal+alunite sedimentary grains in the lahar deposits (S8, S9, S10) represent expulsion of acid-altered materials from beneath the lake. Some of the textures are seriate materials similar to those shown in the upper part of **Figure 2c** (from acid-altered outcrop). This sub-population of laharic sedimentary grains reflects subvolcanic, or at least sublacustrine opaline materials, and reached the surface as a burst of material exploded from the bottom of the lake (Origin C).

Glassy Laharic Sedimentary Grains

We suspect that many of the glassy ORP-bearing laharic sedimentary grains were pre-altered, and were also expelled as cold debris (Origin C). Glass compositions in these laharic sedimentary grains tend toward more mafic compositions than the studied pumice lumps (**Figure 6**), hinting that they represent different magma and might not be juvenile in the sense that they were not molten during the climactic events of early 1817. The glass particles are also far less vesicular than the co-erupted pumice. Another intriguing aspect of these glassy grains is the presence within them of rounded cemented aggregates of altered opal-rich sediments (**Figure 7d**, and Figures S14,S15). In nearly all cases, the aggregate occupies only part of the void in which it resides. This implies that it was incorporated while the melt was still in the process of vesiculating. Plausibly, the aggregate could have contributed H_2O to trigger bubble growth, or alternatively it could have served merely as a convenient site for nucleation. The aggregates resemble the descriptions of Kawah Ijen lake sediments described by Delmelle and Bernard (1994) and Takano et al. (2004), with silica phases, anatase, and barite. We speculate that these cemented sediments were incorporated into erupting andesitic melt prior to 1817 (similar to Origin B). The glassy sediments, along with opal/alunite alteration were then later expelled from the lake in 1817 (Origin C).

The timing of magmatic incorporation of the aggregates by andesitic melt is unknown. Though the andesite could have been emplaced and quenched years earlier, it is also possible that it ascended in the very earliest part of the 1817 magmatic eruption. Some of the lahar was emplaced about 10 days after the start of the eruption, so it is possible that a significant amount of alteration could have taken place at the lake bottom by deep lake water over the intervening time (lake-bottom temperatures are ∼50°C as measured over the past century; Delmelle and Bernard, 1994; Takano et al., 2004; Caudron et al., 2015). Further mudflows were emplaced as late as mid-February. It is unclear when the sampled lahar sediments were deposited, though they were obtained near the top of the deposit, and may represent materials erupted later in the sequence of events.

Availability of Acid and Reactivity of Glass

Though Origin D is our preferred explanation for the majority of ORP, one confounding aspect of this hypothesis is that pumice samples from all over Ijen were inspected and found to contain ORP (Figure S1). Some of these sampling localities are not near the Banyu Pahit and are unlikely to have seen significant amounts of infiltrating acid water during the past 200 years post-eruption. Plausibly, co-eruption of acid lake water, together with pumice and debris contributed sufficient acid into the muddy 1817 deposits to allow for protracted water-rock reaction that created post-eruption pseudomorphs within the phenocryst population in the pumice. Alteration at this time would also have been aided by the elevated temperatures of this material.

One additional factor might be the presence of erupted native sulfur, which is ubiquitous on Kawah Ijen, floating as vesicular mats on the lake, likely sourced from a sulfur pool on the lake floor, and forming mineable sulfur in cooling fumaroles (Van Gelder and Caron, 1915; Delmelle and Bernard, 1994; Takano et al., 2004). After the 1817 eruption, the Banyuwangi Plain was covered in sulfur-bearing mud (Caudron et al., 2015), and acid springs are present on the northern crater rim of Kawah Ijen sourced from native sulfur-bearing phreatic sediments (Figure S1). Surprisingly, we found no direct evidence for native sulfur in the Ijen pumices or laharic sediments during EDS analysis of the Ijen eruption products. Perhaps the presence of sulfur-oxidizing bacteria (e.g., Sulfolobus: Brock et al., 1972) has converted much of the native sulfur that was present in the original sediments, fallout, and flood deposits, creating a local source of sulfuric acid that enabled some of the post-eruption, acid-alteration.

Speculations on the Connection between Phreatomagmatic Activity and Acid Alteration

As mentioned above, amorphous opaline materials (sometimes including ORP) are commonly described in the debris emitted during magmatic-hydrothermal and phreatomagmatic eruptions. The common presence of opaline debris in tephra suggests that acid-altered minerals and related fluids may become highly unstable when heated by encroachment of magma.

Opal and most other advanced argillic alteration products are highly water-rich. Opal itself can contain up to 15 wt% H_2O (Tanner et al., 2015). Kaolinite contains about 14 wt% H_2O as do many other clays found in the advanced argillic environment. Alunite contains about 13 wt% H_2O. All of these hydrous materials are unstable and will dehydrate upon heating. For any such alteration product with 13 wt.% H_2O, devolatilization at 5 MPa (500 m depth at hydrostatic pressure) could generate about 10 cubic meters of steam for each cubic meter of rock. This assumes a rock density of 2,000 kg/m^3 and that the steam is created at the boiling point of water at 5 MPa, which is 264°C. If the magma was able to heat the steam further, greater volumes of steam would be created. Depending on the permeability of the overlying rocks, significant overpressures might be generated by even partial thermal decomposition of hydrous alteration products.

The presence of any interstitial fluid will create further potential for generation of steam. For example, if the rock contains 10% fluid-filled porosity, which is common for acid alteration (Mayer et al., 2016), then ∼27% of the total water in the system is from hydrothermal fluid, with the bulk coming from the hydrous alteration itself. The main point is that the

effect of thermal pressurization due to magmatic intrusion will be up to four times greater in acid-altered rock than in unaltered volcanic terrain containing water-saturated lavas, pyroclastic rocks, etc. Moreover, advanced argillic environments are by nature almost always at elevated temperatures beneath active volcanoes. Their existence is predicated on condensation of sulfur-bearing volcanic gas that inevitably heats the subvolcanic environment. Any new intrusion of magma will therefore disturb a hydrothermal system that is already at elevated temperature such that additional heat will destabilize hydrous minerals, and engender vaporization of near-boiling fluids. The latter process, also known as steam-flashing, is known to increase fragmentation energy (Mayer et al., 2015). Moreover, acid alteration weakens rocks, and increases their porosity and permeability, making them much more prone to fragmentation (Mayer et al., 2016). Explosions will be more likely when pressure increases faster than it can diffuse through the volcanic edifice, and any overlying crater lake.

Pressurization could also be enhanced due to the presence of liquid sulfur, which can clog rock pores. When heated above 159°C, its viscosity increases by over four orders of magnitude, further decreasing permeability and enhancing pressurization (Scolamacchia and Cronin, 2016).

One illustrative example of the relevance of opal-rich materials in the source region of magmatic-hydrothermal eruptions can be seen at the highly scrutinized recent example from Mt. Ontake (Japan) in 2014 (Yamaoka et al., 2016). Dry and wet explosions resulted in widespread generation of ballistic debris, pyroclastic density currents and a lahar whose mud-rich waters were disgorged from within the volcano. Silica is ubiquitous in the eruptive products, and nearly all erupted materials were hydrothermally altered (Minami et al., 2016). The authors did not attempt to differentiate the specific form of amorphous or crystalline silica, but figures clearly show the presence of pseudomorphic replacement of volcanic textures with silica. Though the event was purely hydrothermal in that no juvenile material was erupted, there is considerable geochemical evidence that magmatic input was involved in the triggering of hydrothermal fluid migration. Gas samples over 10 years indicated a progression of He isotopes toward increasingly magmatic values prior to the 2014 event (Sano et al., 2015). Immediately after the eruption, SO_2 emission rates of >2,000 t/d were measured, and rapidly decreased thereafter, though hydrothermal H_2S emissions continued (Mori et al., 2016). It appears likely that the eruption was at least partially triggered by input of magmatic gas at the base of the acid-altered hydrothermal system (Sano et al., 2015; Mori et al., 2016; Yamaoka et al., 2016).

In this example from Ijen, the opaline materials may be somewhat dehydrated, as is consistent with the very low δD of the studied samples and some photomicrographs. Nevertheless, we have no direct evidence that dehydration of advanced argillic minerals caused the 1817 eruptions, or contributed significantly to the explosivity of the eruptions. We merely point out that introduction of magma into a shallow volcanic environment may serve to destabilize any acid-altered materials in a hydrothermal system.

CONCLUSIONS

Our study represents an initial description of the remarkable occurrence of opal-replaced phenocrysts within glassy pumices and particles present in laharic sediments at the surface and subsurface of Kawah Ijen volcano in Indonesia.

Our findings indicate that no single process was responsible for the incorporation of acid-altered materials and sediment in the 1817 eruptive products. Instead, multiple pathways contribute to the presence of amorphous opal (opal-A) in pumice and laharic sediments. (1) *Incorporation of opaline materials in erupting magma*: Micro-xenoliths of cemented opal-bearing sediment (**Figure 7c** and Figure S5) are found within dacitic glass in Ijen pumice, and were almost certainly incorporated into silicate melt during pre- or syn-eruptive ascent. Layered opaline silica is also found as xenoliths in fresh pumice (**Figures 7a,b**). Preservation of opal-A requires quenching of the pumice within a matter of minutes, either by incorporation of cold sediments or immediate eruption. (2) *Post-eruption and post-depositional alteration:* It remains likely that most pumice and laharic sediments were altered after eruption and emplacement at the surface. We have demonstrated that the acidity of Banyu Pahit creek water is sufficiently strong to initiate replacement of plagioclase and pyroxene by opal-A at ambient temperatures. Within the Banyu Pahit drainage, intermittent flow and seepage of acid water through the laharic deposits is possible and could account for many of the ORP. At other locations on Kawah Ijen, post-eruption formation of ORP would have to be instigated by co-erupted lake water or acid-rich muddy deposits co-erupted with the pumice. (3) *Sub-lacustrine alteration of glassy sediments and pumice*: Opal-dominated clasts without associated glass represent ∼10% of the sediments found in the 1817 laharic deposits, and are interpreted as sub-lacustrine sediments ejected during the eruption. Co-deposited glassy sediments in the lahar deposits contain ubiquitous opal-replaced phenocrysts. Glass compositions are more mafic than those found in any studied co-erupted pumice. We suspect that many of the ORP found in glassy sediments were formed prior to the 1817 eruption at the bottom of the lake. Whether these volcanic materials were emplaced beneath the lake early in 1817, or at an earlier time, is unknown. Xenoliths of opal-rich aggregates within the glassy sediment would then in turn indicate syn-eruptive incorporation of altered sediments prior to the 1817 eruption.

Advanced argillic rock types are universally hydrous and yet unstable upon heating. Their consistent presence in phreatomagmatic and magma-hydrothermal deposits at arc volcanoes testifies to the highly unstable nature of acid-altered volcanic edifices. We conclude that breakdown of opal and other ubiquitous hydrous minerals may contribute to the thermal pressurization that occurs when magma intrudes shallow, acid-altered hydrothermal environments.

AUTHOR CONTRIBUTIONS

JL, VvH, KB, and HW co-discovered the opal pseudomorphs and collaboratively explored the phenomena. JL wrote the manuscript and produced most figures. ML collected all high-solution

SEM images and Raman data and assisted in interpretation. KI undertook the high-temperature experiments, VvH the low-temperature acid experiments, and IB collected isotopic data.

FUNDING

Our work is funded by the USGS Volcano Hazards Program and the Volcano Disaster Assistance Program funded jointly by the USGS and the USAID U.S. Office of Foreign Disaster Assistance.

ACKNOWLEDGMENTS

We thank Suparjan and Peter Kelly for collecting samples 1 year after the initial field campaign. Leslie O'Brien assisted with the SEM and electron microprobe. Juliet Ryan-Davis undertook the XRD analysis. Ben Hankins prepared some of the microprobe mounts. Tom Sisson exhibited persistent skepticism that helped guide our efforts to characterize these samples. Dave John, Rafaello Cioni, Pierre Delmelle, and Betty Scheu provided helpful reviews. Any use of trade, firm, or product names is for descriptive purposes only and does not imply endorsement by the U.S. Government.

SUPPLEMENTARY MATERIAL

The Supplementary Material for this article can be found online at: https://www.frontiersin.org/articles/10.3389/feart.2018.00011/full#supplementary-material

REFERENCES

Africano, F., and Bernard, A. (2000). Acid alteration in the fumarolic environment of Usu volcano, Hokkaido, Japan. *J. Volcanol. Geotherm. Res.* 97, 475–495. doi: 10.1016/S0377-0273(99)00162-6

Berger, B. R., Henley, R. W., Lowers, H. A., and Pribil, M. J. (2014). The lepanto cu-au deposit, Philippines: a fossil hyperacidic lake complex. *J. Volcanol. Geotherm. Res.* 271, 70–82. doi: 10.1016/j.jvolgeores.2013.11.019

Bindeman, I. N. (2008). Oxygen isotopes in mantle and crustal magmas as revealed by single crystal analysis. *Rev. Mineral. Geochem.* 69, 445–478. doi: 10.2138/rmg.2008.69.12

Brock, T. D., Brock, K. M., Belly, R. T., and Weiss, R. L. (1972). *Sulfolobus*: a new genus of sulfur-oxidizing bacteria living at low pH and high temperature. *Arch. Mikrobiol.* 84, 54–68. doi: 10.1007/BF00408082

Browne, P. R. L., and Lawless, J. V. (2001). Characteristics of hydrothermal eruptions, with examples from New Zealand and elsewhere. *Earth Sci. Rev.* 52, 299–331. doi: 10.1016/S0012-8252(00)00030-1

Caudron, C., Syabhana, D. K., Lecocq, T., van Hinsberg, V., McCausland, W., Triantafyllou, A., et al. (2015). Kawah Ijen volcanic activity: a review. *Bull. Volcanol.* 77, 16. doi: 10.1007/s00445-014-0885-8

Christenson, B. W., Reyes, A. G., Young, R., Moebis, A., Sherburn, S., Cole-Baker, J., et al. (2010). Cyclic processes and factors leading to phreatic eruption events: insights from the 25 September 2007 eruption through Ruapehu Crater Lake, New Zealand: *J. Volcanol. Geotherm. Res.* 191, 15–32. doi: 10.1016/j.jvolgeores.2010.01.008

Christenson, B. W., and Wood, C. P. (1993). Evolution of a vent-hosted hydrothermal system beneath Ruapehu crater lake, New Zealand. *Bull. Volcanol.* 55, 547–565. doi: 10.1007/BF00 301808

Day, R., and Jones, B., (2008). Variations in water content in opal-A and opal-CT from geyser discharge aprons. *J. Sed. Res.* 78, 301–315.

Delmelle, P., and Bernard, A. (1994). Geochemistry, mineralogy and chemical modeling of the acid crater lake of Kawah Ijen Volcano, Indonesia: *Geochim. Cosmochim. Acta* 58, 2445–2460. doi: 10.1016/0016-7037(94)90023-X

Delmelle, P., Bernard, A., Kusakabe, M., Fischer, T. P., and Takano, B. (2000). Geochemistry of the magmatic-hydrothermal system of Kawah Ijen volcano, East Java, Indonesia. *J. Volcanol. Geothermal. Res.* 97, 31–53. doi: 10.1016/S0377-0273(99)00158-4

Delmelle, P., Helney, W., Opfergelt, S., and Detienne, M. (2015). "Summit acid crater lakes and flank instability in composite volcanoes" in *Volcanic Lakes, Advances in Volcanology*, eds D. Rouwet, B. Christenson, F. Tassi, and J. Vandemeulebrouck (Berlin; Heidelberg: Springer-Verlag), 289–305.

Dobson, P. F., Epstein, S., and Stolper, E. M. (1989). Hydrogen isotope fractionation between coexisting vapor and silicate glasses and melts at low pressure. *Geochim. Et. Cosmochim. Acta* 53, 2723–2730. doi: 10.1016/0016-7037(89)90143-9

Fournier, R. O., and Rowe, J. J. (1966). The deposition of silica in hot springs. *Bull. Volcanol.* 29:585. doi: 10.1007/BF02597179

Gaunt, H. E., Bernard, B., Hidalgo, S., Proaño, A., Wright, H., Mothes, P., et al. (2016). Juvenile magma recognition and eruptive dynamics inferred from the analysis of time series: the 2015 reawakening of Cotopaxi volcano. *J. Volcanol. Geotherm. Res.* 328, 134–146. doi: 10.1016/j.jvolgeores.2016.10.013

Graetsch, H., Flörke, O. W., and Miehe, G. (1985). The nature of water in chalcedony and opal-c from Brazilian agate geodes. *Phys Chem Miner.* 12, 300–306.

Handley, H. K., Macpherson, C. G., Davidson, J. P., Berlo, K., and Lowry, D. (2007). Constraining fluid and sediment contributions to subduction-related magmatism in Indonesia: Ijen Volcanic Complex. *J. Petrol.* 48, 1155–1183. doi: 10.1093/petrology/egm013

Hartwig, C. M., and Rahn, L. A. (1977). Bound hydroxyl in vitreous silica. *J. Chem. Phys.* 67, 4260–4261.

Hedenquist, J. W., Aoki, M., and Shinohara, S. (1994). Flux of volatiles and ore-forming metals from the magma-hydrothermal system of Satsuma Iwojima volcano. *Geology* 22, 585–588.

Hedenquist, J. W., Arribas, Jr. A., and Reynolds, T.J. (1998). Evolution of an intrusion-centered hydrothermal system: far Southeast-lepanto porphyry and epithermal cu-au deposits, Philippines. *Econ. Geol.* 93, 373–404. doi: 10.2113/gsecongeo.93.4.373

Hedenquist, J. W., and Lowenstern, J. B. (1994). The role of magmas in the formation of hydrothermal ore deposits. *Nature* 370, 519–527. doi: 10.1038/370519a0

Hedenquist, J. W., and Taran, Y. A. (2013). Modeling the formation of advanced argillic lithocaps: volcanic vapor condensation above porphyry intrusions. *Econ. Geol.* 108, 1523–1540. doi: 10.2113/econgeo.108.7.1523

Hemley, J. J., and Jones, W. R. (1964). Chemical aspects of hydrothermal alteration with emphasis on hydrogen metasomatism. *Econ. Geol.* 59, 538–569. doi: 10.2113/gsecongeo.59.4.538

Henley, R. W. (2015). "Hyperacidic volcanic lakes, metal sinks and magmatic gas expansion in arc volcanoes," in *Volcanic Lakes, Advances in Volcanology,* eds D. Rouwet, B. Christenson, F. Tassi, and J. Vandemeulebrouck (Berlin; Heidelberg: Springer-Verlag), 155–178.

Henley, R. W., and McNabb, A. (1978). Magmatic vapor plumes and ground-water interaction in porphyry copper emplacement. *Econ. Geol.* 73, 1–20. doi: 10.2113/gsecongeo.73.1.1

Herrington, R. J., and Wilkinson, J. J. (1993). Colloidal gold and silica in mesothermal vein systems. *Geology* 21, 539–542. doi: 10.1130/0091-7613(1993)021<0539:CGASIM>2.3.CO;2

Jones, J. B., and Segnit, E. R. (1971). The nature of opal I. nomenclature and constituent phases. *J. Geol. Soc. Austr.* 18, 57–68.

Kemmerling, G. L. L. (1921). *Het Idjen Hoogland. De Geologie En Geomorphologie van den Idjen. Koninklijke Natuurkundige Vereeniging Monografie II.* Weltevreden-Batavia: G. Kolff & Co.

King, H. E., Plumper, O., Geisler, T., and Putnis, A. (2011). Experimental investigations into the silicification of olivine: implications for the reaction mechanism and acid neutralization. *Am. Miner.* 96, 1503–1511. doi: 10.2138/am.2011.3779

Kita, I., Taguchi, S., and Matsubaya, O. (1985). Oxygen isotope fractionation between amorphous silica and water at 34-93 °C. *Nature* 314, 63–64. doi: 10.1038/314083a0

Loewen, M., and Bindeman, I. N. (2015). Oxygen isotope and trace element evidence for three-stage petrogenesis of the youngest episode (260-79 ka) of Yellowstone rhyolitic volcanism. *Contrib. Mineral. Petrol.* 170:39. doi: 10.1007/s00410-015-1189-5

Lynne, B. Y., Campbell, K. A., Perry, R. S., Browne, P. R. L., and Moore, J. (2006). Acceleration of sinter diagenesis in an active fumarole, Taupo volcanic zone, New Zealand. *Geology* 34, 749–752. doi: 10.1130/G22523.1

Mayer, K., Scheu, B., Gilg, H. A., Heap, M. J., Kennedy, B. M., Lavalee, Y., et al. (2015). Experimental constraints on phreatic eruption processes at Whakaari (White Island volcano). *J. Volcanol. Geotherm. Res.* 302, 150–162. doi: 10.1016/j.jvolgeores.2015.06.014

Mayer, K., Scheu, B., Montanaro, C., Yilmaz, T. I., Isaia, R., Aßbichler, D., et al. (2016). Hydrothermal alteration of surficial rocks at Solfatara (Campi Flegrei): petrophysical properties and implications for phreatic eruption processes. *J. Volcanol. Geotherm. Res.* 320, 128–143. doi: 10.1016/j.jvolgeores.2016.04.020

McCollom, T. M., Robbins, M., Moskowitz, B., Berquo, T. S., Jöns, N., and Hynek, B. M. (2013). Experimental study of acid-sulfate alteration of basalt and implications for sulfate deposits on Mars. *J. Geophys. Res. Planets* 118, 577–614, doi: 10.1002/jgre.20044

McMillan, P. (1984). Structural studies of silicate glasses and melts-applications and limitations of Raman spectroscopy. *Am. Miner.* 69, 622–644.

Minami, Y., Imura, T., Hayashi, S., and Ohba, T. (2016). Mineralogical study on volcanic ash of the eruption on September 27, 2014 at Ontake volcano, central Japan: correlation with porphyry copper systems. *Earth Planets Space* 68:67. doi: 10.1186/s40623-016-0440-2

Mori, T., Hashimoto, T., Terada, A., Yoshimoto, M., Kazahaya, R., Shinohara, S., et al. (2016). Volcanic plume measurements using a UAV for the 2014 Mt. Ontake eruption. *Earth Planets Space* 68:49. doi: 10.1186/s40623-016-0418-0

Nolan, G., and Bindeman, I. N. (2013). Experimental investigation of rates and mechanisms of isotope exchange (O, H) between volcanic ash and isotopically-labeled water. *Geochim. Cosmochim. Acta* 111, 5–27. doi: 10.1016/j.gca.2013.01.020

Rodgers, K. A., Brownebc P. R. L., Buddleb, T. F., Cookd, K. L., Greatrex, R. A., Hampton, W. A. et al. (2004). Silica phases in sinters and residues from geothermal fields of New Zealand. *Earth Sci. Rev.* 66, 1–61. doi: 10.1016/j.earscirev.2003.10.001

Rodríguez, A., and van Bergen, M. J. (2017). Superficial alteration mineralogy in active volcanic systems: an example of Poás volcano, Costa Rica. *J. Volcanol. Geotherm. Res.* 346, 54–80. doi: 10.1016/j.jvolgeores.2017.04.006

Sano, Y., Kagoshima, T., Takahata, N., Nishio, Y., Roullearu, E., Pinti, D. L., et al. (2015). Ten-year helium anomaly prior to the 2014 Mt Ontake eruption. *Sci. Rep.* 5:13069. doi: 10.1038/srep13069

Scher, S., Williams-Jones, A. E., and Williams-Jones, G. (2013). Fumarolic activity, acid-sulfate alteration and high sulfidation epithermal precious metal mineralization in the crater of Kawah Ijen Volcano, Java, Indonesia. *Econ. Geol.* 108, 1099–1118 doi: 10.2113/econgeo.108.5.1099

Schipper, C. I., and White, J. D. L. (2016). Magma-slurry interaction in Surtseyan eruptions. *Geology* 44, 195–198. doi: 10.1130/G37480.1

Scolamacchia, T., and Cronin, S. J. (2016). Idiosyncrasies of volcanic sulfur viscosity and the triggering of unheralded volcanic eruptions. *Front. Earth Sci.* 4:24. doi: 10.3389/feart.2016.00024

Shinohara, H. (2009). A missing link between volcanic degassing and experimental studies on chloride partitioning. *Chem. Geol.* 263, 51–59 doi: 10.1016/j.chemgeo.2008.12.001

Sitorus, K. (1990). *Volcanic stratigraphy and geochemistry of the Idjen Caldera Complex, East-Java, Indonesia*. Ph.D. thesis, Victoria University of Wellington.

Symonds, R. B., Rose, W. I., Bluth, G. J. S., and Gerlach, T. M. (1994). "Volcanic-gas studies: methods, results, and applications," in *Volatiles in Magmas, Reviews of Mineralogy,* Vol. 30, eds M. R. Carrol and J. R. Holloway (Washington, DC: Mineralogical Society of America), 1–66.

Takano, B., Suzuki, K., Sugimori, K., Ohba, T., Fazlullin, S. M., Bernard, A., et al. (2004). Bathymetric and geochemical investigation of Kawah Ijen Crater Lake, East Java, Indonesia. *J. Volcanol. Geotherm. Res.* 135, 299–329. doi: 10.1016/j.jvolgeores.2004.03.008

Tanner, D., Henley, R. W., Mavrogenes, J. A., Holden, P., and Mernagh, T. P. (2015). Silica hydrate preserved with d18O-rich quartz in high-temperature hydrothermal quartz in the high sulfidation copper-gold deposit at El Indio, Chile: *Chem. Geol.* 391, 90–99. doi: 10.1016/j.chemgeo.2014.11.005

Van Gelder, J. K., and Caron, M. H. (1915). "Den Zwavelafzettingen in Den Kawah Idjen," in *Jaarboek van Het Mijnwezen in Nederlandsch Indie* (Verhandelingen, Tweede Gedeelte), 70–90.

van Hinsberg, V., Berlo, K., Sumarti, S., van Bergen, M., and Williams-Jones, A. (2010b). Extreme alteration by hyperacid brines at Kawah Ijen volcano, East Java, Indonesia: II Metasomatic imprint and element fluxes. *J. Volcanol. Geotherm. Res.* 196, 169–184. doi: 10.1016/j.jvolgeores.2010.07.004

van Hinsberg, V., Berlo, K., van Bergen, M. J., and Williams-Jones, A. E. (2010a). Extreme alteration by hyperacidic brines at Kawah Ijen volcano, East Java, Indonesia: I. Textural and mineralogical imprint. *J. Volcanol. Geotherm. Res.* 198, 253–263. doi: 10.1016/j.jvolgeores.2010.09.002

van Hinsberg, V., Vigouroux, N., Palmer, S., Berlo, K., Mauri, G., Williams-Jones, A., et al. (2015). "Element flux to the environment of the passively degassing crater lake-hosting Kawah Ijen volcano, Indonesia, and implications for estimates of the global volcanic flux," in *Geochemistry and Geophysics of Active Volcanic Lakes,* eds T. Ohba, B. Capaccioni, and C. Caudron (London: Geological Society London Special Publication), 437.

Williamson, B. J., Wilkinson, J. J., Luckham, P. F., and Stanley, C. J. (2002). Formation of coagulated colloidal silica in high-temperature mineralizing fluids. *Miner. Mag.* 66, 547–553. doi: 10.1180/0026461026640048

Wood, C. P. (1994). Mineralogy at the magma-hydrothermal system interface in andesite volcanoes, New Zealand. *Geology* 22, 75–78. doi: 10.1130/0091-7613(1994)022<0075:MATMHS>2.3.CO;2

Woudstra, H. (1921). *Analyse van merkwaardige water- Soorten Op Het Idjen-Hoogland. Koninklijke Natuurkundige Vereeniging Monografie II*. Weltevreden-Batavia: G. Kolff & Co.

Yamaoka, K., Geshi, N., Hashimoto, T., Ingebritsen, S. E., and Oikawa, T. (2016). Special issue "The phreatic eruption of Mt. *Ontake volcano in 2014*". *Earth Planets Space* 68, 175. doi: 10.1186/s40623-016-0548-4

Conflict of Interest Statement: The authors declare that the research was conducted in the absence of any commercial or financial relationships that could be construed as a potential conflict of interest.